The repression of full-length RIG-I can be liberated upon its encounter with viral RNA. Thus, the de-repression mechanism is critical for the function of RIG-I for acting as a sensor and a switch for signaling. CTD binds to dsRNA with its basic cleft [10]; thus, its involvement in RNA recognition is suggested. It is presumed that the helicase domain also participates in viral RNA recognition, since full-length RIG-I exhibits higher RNA binding affinity [10,11]. Binding of dsRNA induces ATPase activity of RIG-I in vitro. ATPase-deficient RIG-I acts as a dominant inhibitor [5], suggesting that ATP binding and/or its hydrolysis is a critical step in de-repression. RIG-I is a functional RNA helicase, which consumes ATP for dsRNA unwinding [10]; however, dsRNA substrates resistant to RIG-I helicase activity, but not those susceptible, induce IFN production, suggesting that dsRNA unwinding is not critical for signaling. Therefore it is hypothesized that ATPase activity of RIG-I induces a conformational change, resulting in unmasking CARD. Once CARD is liberated, RIG-I may undergo oligomeric complex formation [9]. The oligomer also recruits another CARD-containing adaptor, IPS-1 (IFN-β promoter stimulator 1) (also known as MAVS, VISA and Cardif, [12–15]). IPS-1 is a unique signaling adaptor, expressed on the outer membrane of mitochondria, and its specific localization is critical for its function [13]. IPS-1 transmits a signal through TRAF proteins, resulting in transcription factors IRF-3, IRF-7 and NF-κB, which are responsible for the activation of IFN and cytokine genes [16].

Repression of RIG-I in uninfected cells is crucial for tight regulation of the host immune system and prevents unwanted production of IFN under ordinary conditions; however, the precise mechanism of auto-repression is not known and there is no evidence for the existence of "active" and "inactive" conformations. In the current study, we further delimited RD to the 55 amino acid linker between the helicase domain and CTD. Mutant RIG-I containing amino acid substitutions within the linker conferred constitutive activity. Furthermore, trypsin digestion of wild-type and mutant RIG-I revealed a distinct conformation, suggesting that the mutation inactivated RD and induced an "open" conformation. These findings shed light on the role of RD in RIG-I regulation.

2. Materials and methods

2.1. Cell culture

HEK293T, Huh7.5 and Huh7 cells were maintained in Dulbecco's modified Eagle's medium (DMEM) supplemented with 10% fetal bovine serum (FBS) and 1% penicillin–streptomycin.

2.2. Plasmid construction

All RIG-I full-length mutant constructs used in this study were generated with Prime Star (R) HS DNA Polymerase (TAKARA, Shiga, Japan) or the KOD-Plus Mutagenesis Kit (TOYOBO LIFE SCIENCE, Osaka, Japan), using primers containing the desired mutation, and were sequenced using an ABI 3130xl automatic DNA sequencer to verify the presence of the mutation.

2.3. Protein sequence alignment

Multiple protein sequence alignment was performed using the ClustalX program [17]. DSC, MLRC, and PHD methods were used to predict the protein secondary structure of the linker sequences on the NPS@ (Network Protein Sequence Analysis) server [18].

2.4. Protein purification

The cDNA encoding fusion protein, consisting of Flag-tag and human RIG-I or mutants, was inserted into pAcGHLT-B vector (BD Biosciences, CA, USA), which has GST and His-tag, between NcoI and SmaI sites. To obtain recombinant baculoviruses, SF9 insect cells were co-transfected with the expression plasmid and BD Baculo Gold Linearized Baculovirus DNA (BD Biosciences) according to the manufacturer's protocol. Recombinant virus was recovered from the culture supernatant. The recombinant RIG-I proteins were expressed in Sf9 or High five insect cells (2×10^7 cells/150 mm dish) by infection with recombinant baculovirus (moi 10) for 4 days. The cells were lysed in lysis buffer (50 mM Tris–HCl pH 8.0, 150 mM NaCl, 1.5 mM DTT, 1% Triton X-100) with protease inhibitor cocktail (Nacalai Tesque, Kyoto, Japan). The lysates were centrifuged at 15,000 rpm for 20 min. The supernatants were mixed with Ni-NTA super-flow (QIAGEN, Hilden, Germany) and the beads were washed with binding buffer (20 mM imidazole, 50 mM Tris–HCl pH 8.0, 150 mM NaCl, 1.5 mM DTT). Proteins were eluted with elution buffer 1 (500 mM imidazole, 50 mM Tris–HCl pH 8.0, 150 mM NaCl, 1.5 mM DTT). The eluted protein was further purified with glutathione Sepharose 4B (GE Healthcare, Little Chalfont, Buckinghamshire, UK). Bound proteins were washed with wash buffer (50 mM Tris–HCl pH 8.0, 150 mM NaCl, 1.5 mM DTT) and eluted with elution buffer 2 (50 mM Tris–HCl pH 8.0, 150 mM NaCl, 20 mM glutathione).

2.5. Immunoblot analysis

Huh7.5 cells were seeded in a 6 cm dish (5×10^5 cells/dish/2 ml medium). Before transfection, culture medium was replaced with serum-free DMEM. Expression plasmid for RIG-I wt or mutants (2 μg) was mixed with 1 ml DMEM and 5 μl polyethylenimine Max (Polysciences, Warrington, PA, USA), and then incubated for 15 min. The mixture was added to the culture. After incubation for 1 h, FBS was added to a final concentration 10%. After harvest, whole cell lysate was prepared with NP40 lysis buffer and subjected to Native PAGE or SDS PAGE as described previously [6,19].

2.6. ATPase assay

Reaction mixture (25 μl: 1 μg purified recombinant RIG-I protein, 100 ng RNA, 20 mM Tris–HCl pH 8.0, 1.5 mM $MgCl_2$, 1.5 mM DTT, 20 units Protector RNase Inhibitor, 1 mM ATP) was incubated at 37 °C for 30 min. The product, inorganic phosphate, was quantified using BioMol Green (Enzo, Farmingdale, NY, USA).

2.7. RNA

25 bp dsRNA was prepared by annealing chemically synthesized complementary RNA (p25/25) as described previously [10]. Then, 5′-triphosphate-containing RNA was synthesized using a DNA template and T7 RNA polymerase as described previously [10] as 5′pppGG25, presumably containing copy-back 3′end. Poly (I:C) pull down assay was performed as described previously [5].

2.8. RNA binding assay

Purified GST-fused RIG-I proteins (5 μg) were mixed with the indicated RNAs (0.1 μg) in a 20 μl reaction mixture (20 mM Tris–HCl pH 8.0, 1.5 mM $MgCl_2$, 1.5 mM DTT) and incubated at 37 °C for 15 min. The mixture was resolved by 15% native PAGE. The gel was stained with EtBr to visualize free RNA and protein/RNA complex.

Please cite this article in press as: M. Kageyama et al., 55 Amino acid linker between helicase and carboxyl terminal domains of RIG-I functions as a critical repression domain and determines inter-domain conformation, Biochem. Biophys. Res. Commun. (2011), doi:10.1016/j.bbrc.2011.10.015

2.9. Luciferase reporter assay

Huh7.5 or Huh7 cells were seeded in a 12-well plate (5×10^4 cells/well/0.5 ml medium). Then, 2 μg p-125 Luc IFN-β luciferase reporter plasmid, 20 ng pRL-tk, and 4 μg expression plasmid for RIG-I wt or mutants were mixed with 150 μl Opti-MEM and 9 μl Fugene 6 (Roche), and incubated for 15 min. The mixture was dispensed into 3 wells (50 μl/well). After 20 h of incubation, cells in each well were split into two wells for virus infection. After cells had attached to the dish, one well was mock treated and the other well was infected with SeV (moi 1) for 20 h. Cells were subjected to a Dual-Luciferase (R) Reporter Assay System (Promega, Madison, WI, USA). Luciferase activity was normalized using Renilla luciferase activity (pRL-tk) as a reference. The values show relative

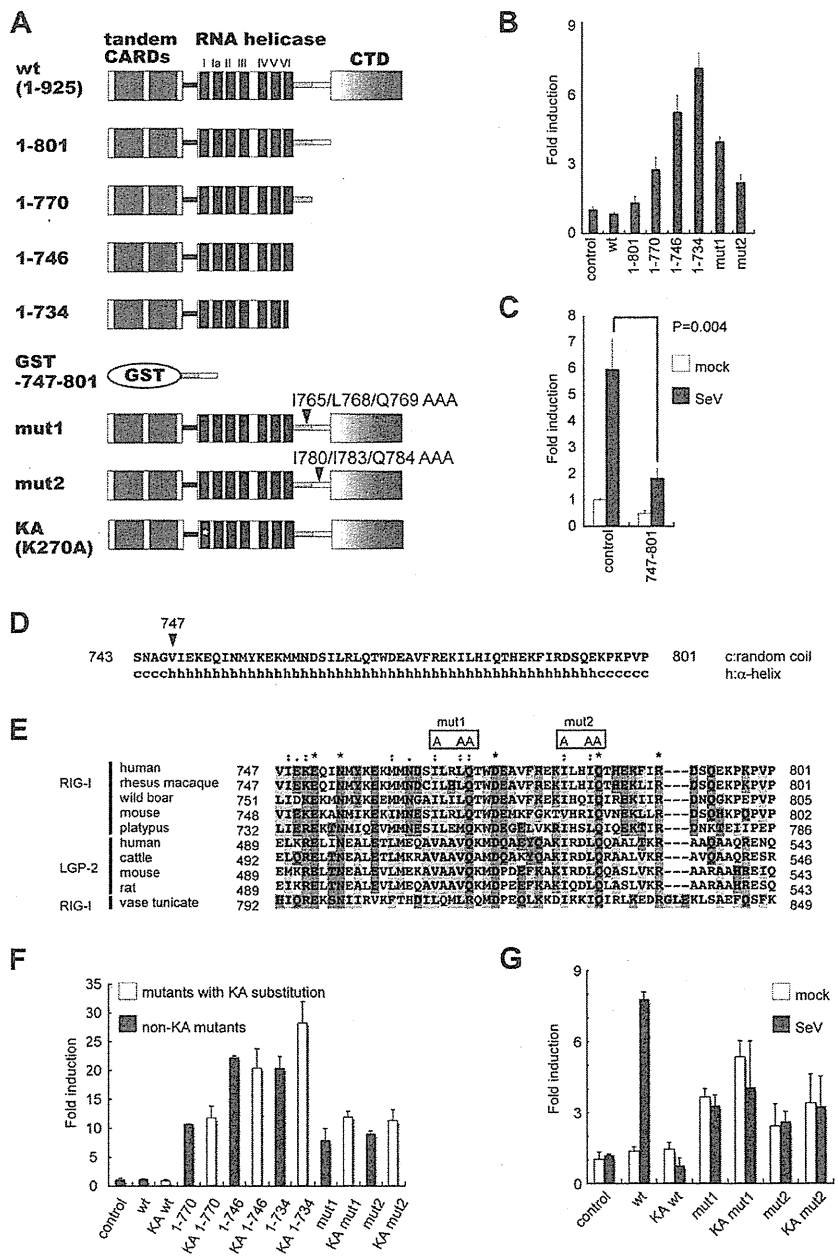

Fig. 1. RIG-I 747-801 is the minimal repression domain. (A) Domain structure of the RIG-I constructs used in this study. The amino acid region encoded by each construct is shown on the left. Mutations are indicated by arrows. (B and C) Activation of IFN-β promoter by RIG-I wt and mutants. Huh7.5 (B) or Huh7 cells (C) were transfected with indicated expression vectors, IFN-β luciferase reporter and pRL-tk as the internal control. In C, 52 h after transfection, cells were infected with Sendai virus (SeV) for 20 h. 24 h (B) or 72 h (C) after transfection, the cells were harvested, and cell lysates were subjected to dual luciferase assay. The values (*Y* axis) show relative luciferase activity as fold induction normalized by the value of unstimulated cells transfected with empty vector (control) for each experiment. Data represent the mean ± standard deviations (SD) ($n = 3$). (D) Predicted secondary structure of the linker of RIG-I. (E) Multiple sequence alignment of the linker of RIG-I and LGP2 from different species. The sequences were aligned using the ClustalX program. Invariant residues are marked with an asterisk. Highly conserved residues are marked with a colon. Similar residues are marked with a dot. Residues targeted for mutation are indicated at the top and were substituted with alanine, indicated as A. (F and G) The effect of ATP binding site mutation on the activity of RIG-I and mutants. Huh7.5 cells were transfected with the indicated expression vectors in the presence of the luciferase reporter and pRL-tk, as in (B). KA: K270A mutation, which disrupts ATP binding motif. 24 h (F) or 72 h (G) after transfection, the cells were harvested. Constitutive activity (F) or SeV induced activity (G) was determined.

Please cite this article in press as: M. Kageyama et al., 55 Amino acid linker between helicase and carboxyl terminal domains of RIG-I functions as a critical repression domain and determines inter-domain conformation, Biochem. Biophys. Res. Commun. (2011), doi:10.1016/j.bbrc.2011.10.015

luciferase activity as fold induction normalized by the value of unstimulated cells transfected with empty vector (control) for each experiment.

2.10. Trypsin digestion

The reaction mixture (10 μl) contained 0.5 picomoles of GST-RIG-I or GST-RIG-I mutants in elution buffer 2. Five nanograms of trypsin (TPCK-treated) was added to the mixture and incubated at 37 °C for 20 min. The reaction was terminated by adding SDS loading buffer (Nacalai Tesque, Kyoto, Japan) (10 μl) and boiling for 1 min. The digestion products were analyzed by SDS–PAGE (5–20% acrylamide gradient) followed by silver staining or Western blotting using monoclonal ANTI-FLAG M2 antibody.

3. Results

3.1. Delimitation of RIG-I repressor domain

Previously, the region of RIG-I encompassing a.a. 735–925 was mapped as RD [9]. Deletion of a.a. 735–925 results in constitutive active RIG-I. Moreover, RD is sufficient to repress virus-induced activation of endogenous RIG-I when a.a. 735–925 alone is over expressed. a.a. 735–925 encompasses the entire CTD (a.a. 802–925), which was defined as a structural domain by a protease digestion experiment and contains the RNA-binding basic cleft [10], and a linker (a.a. 747–801) connecting the helicase domain and the CTD (Fig. 1A). To delimit the functional RD further, we prepared detailed deletion mutants of RIG-I and examined their stimulatory activity on IFN-β luciferase reporter (Fig. 1A and B). Without viral stimulus, wt RIG-I exhibited no stimulatory activity. Consistent with the previous report [9], RIG-I1-734 exhibited marked activation of the reporter. Interestingly, RIG-I1-801, which lacks the entire CTD, exhibited little activity; however, partial and complete deletion of the linker (1–770 and 1–746, respectively) exhibited enhanced reporter activity (Fig. 1B), suggesting that the linker is the minimal repression domain. We genarated a GST fusion construct, GST-RIG-I 747-801, in which the linker was connected with GST. Cells expressing GST as a control showed elevated IFN-β promoter activity upon SeV infection which selectively activates RIG-I [20]. (Fig. 1C); however, over-expression of GST-RIG-I747-801 suppressed reporter gene activation upon viral stimulus, suggesting that the newly defined repression domain is capable of acting in *trans*, the feature described for a.a. 735–925. The secondary structure prediction program (Section 2) suggested that a.a. 747–801 is mostly composed of α-helix (Fig. 1D). Alignment of the primary sequence corresponding to linkers of LGP and RIG-I from different species revealed that several amino acids are highly conserved (Fig. 1E); notably, φXXφQ motif (in which φ is I, L or V) is conserved at a.a. 765 and 780 (human RIG-I numbering). We constructed mutants in which each of the motif was disrupted: mutant 1 (ILQ/765, 768, and 769/AAA) and mutant 2 (IIQ/780, 783, and 784/AAA), and analyzed their basal activity. Interestingly, both mutant 1 and 2 promoted reporter gene expression without viral infection (Fig. 1B), consistent with the hypothesis that the linker structure is critical for repression function.

3.2. ATP binding site of RIG-I is required for virus-induced activation of IFN-β promoter but not for constitutive activity of the linker mutants

Because the ATP binding site is indispensable for virus-induced activation of RIG-I [5], we examined whether the constitutive active RIG-I mutants described in Fig. 1B are similarly dependent on ATP binding. We introduced K270A mutation into each of the deletions, mutant 1 and 2 and examined their activity (Fig. 1F). Interestingly, KA mutation did not change the trans-activation potential of the constitutive active mutants. As expected, K270A mutation totally abolished SeV-induced activation of IFN-β promoter by wt RIG-I (Fig. 1G). On the other hand, although mutant 1 and 2 are constitutively active, their activation level was not enhanced by SeV infection in K270 or K270A context. To further confirm whether the constitutive active mutants activate the reporter gene through the activation of IRF-3, we examined IRF-3 dimerization in cells over-expressing wt and mutants (Fig. 2). IRF-3 dimer formation was observed in cells over-expressing constitutively active mutants 1-770, 1-746 and 1-734 (Fig. 2A), and the level of IRF-3 dimer was roughly proportional to the reporter assay (Fig. 1B). Likewise, mutant 1 and 2 induced IRF-3 dimer (Fig. 2B).

3.3. Mutation 1 and 2 within the linker did not affect RNA binding activity of RIG-I

Next, the RNA binding activity of RIG-I mutant 1 and 2 was examined using 25 bp dsRNA (p25/25), 5′ tri-phosphate-containing RNA (5′pppGG25), and poly (I:C) (Fig. 3A and B). Wild-type RIG-I, and mutant 1 and 2 exhibited binding to these RNA. Mutant 1 and 2 bound to 5′ pppGG25 and poly (I:C) with slightly increased efficiency (in repeated experiments, data not shown). These results suggest that mutation within the linker did not cause overall structural distortion and at least preserved the function of RNA recognition.

3.4. Mutation 1 and 2 within the linker disconnected dsRNA binding and ATPase activity of RIG-I

Wild-type RIG-I, and mutant 1 and 2 were produced as GST fusion, purified and subjected to the ATPase assay (Section 2). Although wild-type RIG-I exhibited very low ATPase activity, it was markedly enhanced by 5′ pppGG25 or poly (I:C) (Fig. 3C). In contrast, ATPase activity of mutant 1 and 2 was not increased even

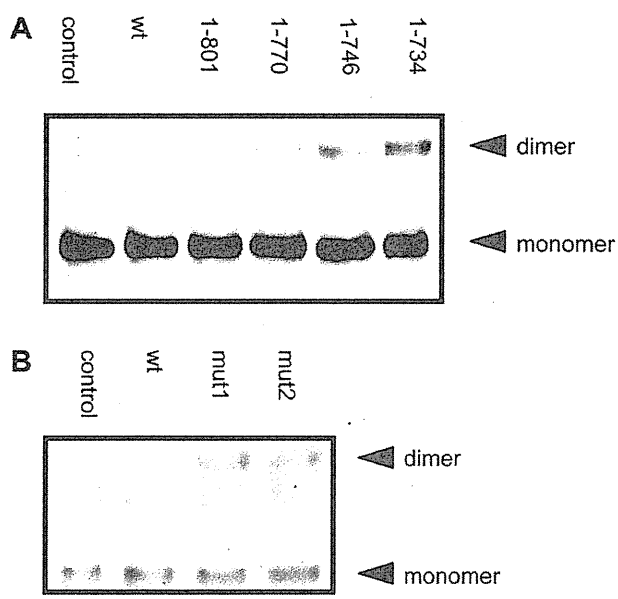

Fig. 2. Linker region of RIG-I regulates the activation of IRF-3. Dimerization of IRF-3 induced by RIG-I mutants. Huh7.5 cells were transfected with empty vector (control), expression vector for Flag-tagged RIG-I wt or indicated mutants. 36 h (A) or 16 h (B) after transfection, cell lysates were subjected to Native PAGE and immunoblot analysis with anti-IRF-3 antibody. IRF-3 monomer and dimer are indicated by arrows.

Please cite this article in press as: M. Kageyama et al., 55 Amino acid linker between helicase and carboxyl terminal domains of RIG-I functions as a critical repression domain and determines inter-domain conformation, Biochem. Biophys. Res. Commun. (2011), doi:10.1016/j.bbrc.2011.10.015

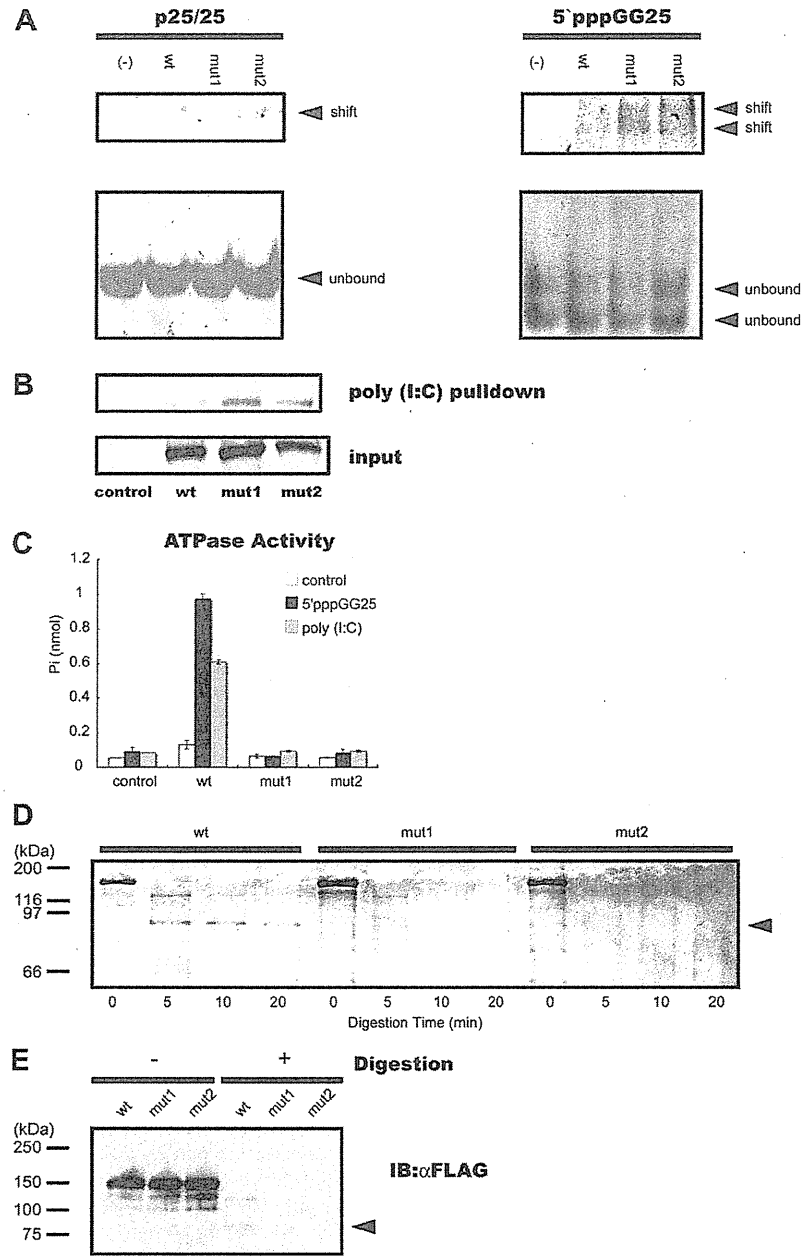

Fig. 3. Characterization of RIG-I mutant protein. (A) RNA-binding activity of RIG-I wt and mutants. Recombinant full-length RIG-I was incubated with p25/25 (left) or 5'pppGG25 (right) and separated by gel electrophoresis (Section 2). Arrows denote the position of unbound RNA (lower) or RNA-RIG-I complex (upper). (B) Poly (I:C) pull-down of RIG-I proteins. Extract from HEK293T cells transfected with empty vector (control), Flag-tagged RIG-I wt or mutant vectors was mixed with poly (I:C)-agarose beads, and subjected to pull-down assay. RIG-I proteins in the input material (lower panel) and recovered from pull-down (upper panel) are shown. (C) ATPase activity of RIG-I. ATPase activity of the recombinant GST-RIG-I proteins was determined as described in Section 2. Data are the mean ± SD ($n = 2$). Similar data were obtained from a separate experiment. (D and E) protease digestion of RIG-I. Recombinant GST-RIG-I proteins were digested with trypsin at 37 °C for the indicated times, resolved by SDS–PAGE and visualized by silver staining (D). Similarly digested RIG-I (for 20 min) was analyzed by immunoblotting with anti-Flag (E).

in the presence of ligands. As both mutant 1 and 2 bind dsRNA similarly to the wild-type (Fig. 3A and B), these mutants are incapable of connecting the dsRNA binding signal to the activation of ATPase. These results suggest that mutation 1 and 2 result in altered conformation of RIG-I.

3.5. Conformational change of RIG-I induced by mutation 1 and 2

To investigate the conformational change of RIG-I, we subjected wild-type RIG-I and mutants to limited trypsin digestion and analyzed the digested product by SDS–PAGE (Fig. 3D). Trypsin digestion of wild-type RIG-I generated an intermediate RIG-I fragment of 90 kD after 5 min of digestion. This fragment persisted at least until 20 min of digestion, suggesting that it is relatively resistant to this protease. Western blotting using anti-Flag antibody, whose epitope is attached at the amino terminus of the RIG-I construct, revealed that the 90 kD fragment contains the intact Flag epitope attached to the N-terminus of RIG-I (Fig. 3E). Notably, the result suggests that the CARD was protected from digestion. From the calculated molecular mass of the fragment, we mapped the cleav-

Please cite this article in press as: M. Kageyama et al., 55 Amino acid linker between helicase and carboxyl terminal domains of RIG-I functions as a critical repression domain and determines inter-domain conformation, Biochem. Biophys. Res. Commun. (2011), doi:10.1016/j.bbrc.2011.10.015

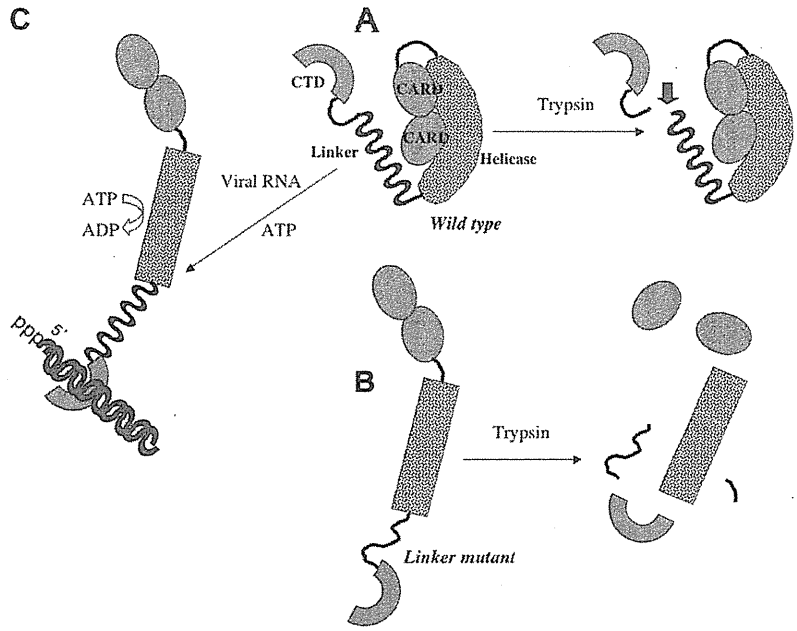

Fig. 4. Model for basal repression and de-repression of RIG-I. Schematic model of RIG-I suppression by its linker region and de-repression by viral RNA is shown. Tandem CARDs and domains encoding the helicase, linker and CTD are shown. The linker repressed RIG-I signaling by masking CARDs in the absence of viral RNA (A). Trypsin digestion partially digested RIG-I, resulting in digestion-resistant fragment consisting of CARD and helicase domain. Linker mutation changes the linker structure, resulting in the open conformation, in which CARD is exposed (B). Mutant 1 and 2 were highly sensitive to trypsin digestion and no resistant fragment was observed. Binding of viral RNA to RIG-I induces ATPase activity, leading to its conformational change, resulting in unmasking of CARD (C).

age site around amino acid 800 of RIG-I and GST was cleaved off. In sharp contrast, neither mutant 1 and 2 exhibited a trypsin-resistant fragment within this range of digestion, strongly suggesting that the conformation of mutant 1 and 2, particularly the complex of CARD and helicase domain, is much less resistant to trypsin digestion.

4. Discussion

In the present work, we demonstrated that the linker, which connects the helicase domain and CTD, is the minimal domain for the repression of constitutive activity of RIG-I. Prediction of the secondary structure suggested that the linker is mostly composed of α-helix. Furthermore, comparison of the primary sequences of the linkers of RIG-I and LGP2 proteins revealed conserved amino acid residues. Mutagenesis of these key amino acids resulted in impaired repression function. We hypothesized a model, described in Fig. 4. Wild-type RIG-I conforms a closed structure so CARD is masked (Fig. 4A); thus, the basal activity of wild-type RIG-I is minimized. Mutation of the linker disrupts the closed conformation and results in the release of CARD. The protease digestion of wild-type and mutant RIG-I strongly suggests a conformational change by linker mutation (Fig. 4B). Interestingly, once such a conformational change is allowed by mutation, ATPase activity is dispensable for signaling (Fig. 1F). This is consistent with the hypothesis that RIG-I CARD is essential for signaling but its availability is strictly regulated by the overall conformation of full-length RIG-I. Our protease digestion experiment demonstrates for the first time that two distinct conformations, repressed (wild-type RIG-I) and de-repressed (mutant RIG-I) exist and that the linker of 55 amino acids is responsible for autorepression.

The autorepression state can be reversed by viral infection through a multiple step mechanism: (i) recognition of non-self RNA, (ii) binding and hydrolysis of ATP, (iii) conformational change and (iv) ubiquitination. The non-self RNA patterns, such as dsRNA and 5′tri-phosphate are recognized by the CTD and helicase domain [10]. RNA binding induces ATPase activity of RIG-I (Fig. 3C), leading to the conformational change (Fig. 4C). In addition, there are several reports that ubiquitination plays an important role in RIG-I activation, although the proposed models are not consistent [21–23]. It is therefore important to determine the repressed and de-repressed conformation of full-length RIG-I at atomic resolution. Such structures will explain how the linker region regulates the overall conformation of the RIG-I molecule.

Acknowledgments

We thank Pro. S. Yonehara for valuable discussion. This work was supported in part by a Grant-in-Aid from the Ministry of Education, Science, Sports and Culture, Japan, the Ministry of Health, Labor and Welfare, the PRESTO Japan Science and Technology Agency, the Uehara Memorial Foundation, Takeda Science Foundation, and Nippon Boehringer Ingelheim.

References

[1] Y.M. Loo, M. Gale, Immune signaling by RIG-I-like receptors, Immunity 34 (2011) 680–692.
[2] M. Schlee, G. Hartmann, The chase for the RIG-I ligand–recent advances, Mol. Ther. 18 (2010) 1254–1262.
[3] O. Takeuchi, S. Akira, Innate immunity to virus infection, Immunol. Rev. 227 (2009) 75–86.
[4] M. Yoneyama, T. Fujita, Recognition of viral nucleic acids in innate immunity, Rev. Med. Virol. 20 (2010) 4–22.
[5] M. Yoneyama, M. Kikuchi, T. Natsukawa, N. Shinobu, T. Imaizumi, M. Miyagishi, K. Taira, S. Akira, T. Fujita, The RNA helicase RIG-I has an essential function in double-stranded RNA-induced innate antiviral responses, Nat. Immunol. 5 (2004) 730–737.
[6] M. Yoneyama, M. Kikuchi, K. Matsumoto, T. Imaizumi, M. Miyagishi, K. Taira, E. Foy, Y.M. Loo, M. Gale, S. Akira, S. Yonehara, A. Kato, T. Fujita, Shared and unique functions of the DExD/H-box helicases RIG-I, MDA5, and LGP2 in antiviral innate immunity, J. Immunol. 175 (2005) 2851–2858.
[7] V. Hornung, J. Ellegast, S. Kim, K. Brzózka, A. Jung, H. Kato, H. Poeck, S. Akira, K.K. Conzelmann, M. Schlee, S. Endres, G. Hartmann, 5′-Triphosphate RNA is the ligand for RIG-I, Science 314 (2006) 994–997.

Please cite this article in press as: M. Kageyama et al., 55 Amino acid linker between helicase and carboxyl terminal domains of RIG-I functions as a critical repression domain and determines inter-domain conformation, Biochem. Biophys. Res. Commun. (2011), doi:10.1016/j.bbrc.2011.10.015

[8] A. Pichlmair, O. Schulz, C.P. Tan, T.I. Näslund, P. Liljeström, F. Weber, C. Reis e Sousa, RIG-I-mediated antiviral responses to single-stranded RNA bearing 5′-phosphates, Science 314 (2006) 997–1001.

[9] T. Saito, R. Hirai, Y. Loo, D. Owen, C. Johnson, S. Sinha, S. Akira, T. Fujita, M.J. Gale, Regulation of innate antiviral defenses through a shared repressor domain in RIG-I and LGP2, Proc. Natl. Acad. Sci. USA 104 (2007) 582–587.

[10] K. Takahasi, M. Yoneyama, T. Nishihori, R. Hirai, H. Kumeta, R. Narita, M.J. Gale, F. Inagaki, T. Fujita, Nonself RNA-sensing mechanism of RIG-I helicase and activation of antiviral immune responses, Mol. Cell 29 (2008) 428–440.

[11] S. Cui, K. Eisenächer, A. Kirchhofer, K. Brzózka, A. Lammens, K. Lammens, T. Fujita, K. Conzelmann, A. Krug, K. Hopfner, The C-terminal regulatory domain is the RNA 5′-triphosphate sensor of RIG-I, Mol. Cell 29 (2008) 169–179.

[12] T. Kawai, K. Takahashi, S. Sato, C. Coban, H. Kumar, H. Kato, K. Ishii, O. Takeuchi, S. Akira, IPS-1, an adaptor triggering RIG-I- and Mda5-mediated type I interferon induction, Nat. Immunol. 6 (2005) 981–988.

[13] R.B. Seth, L. Sun, C.K. Ea, Z.J. Chen, Identification and characterization of MAVS, a mitochondrial antiviral signaling protein that activates NF-kappaB and IRF 3, Cell 122 (2005) 669–682.

[14] L.G. Xu, Y.Y. Wang, K.J. Han, L.Y. Li, Z. Zhai, H.B. Shu, VISA is an adapter protein required for virus-triggered IFN-beta signaling, Mol. Cell 19 (2005) 727–740.

[15] E. Meylan, J. Curran, K. Hofmann, D. Moradpour, M. Binder, R. Bartenschlager, J. Tschopp, Cardif is an adaptor protein in the RIG-I antiviral pathway and is targeted by hepatitis C virus, Nature 437 (2005) 1167–1172.

[16] K. Honda, A. Takaoka, T. Taniguchi, Type I interferon gene induction by the interferon regulatory factor family of transcription factors, Immunity 25 (2006) 349–360.

[17] J.D. Thompson, T.J. Gibson, F. Plewniak, F. Jeanmougin, D.G. Higgins, The CLUSTAL_X windows interface. flexible strategies for multiple sequence alignment aided by quality analysis tools, Nucleic Acids Res. 25 (1997) 4876–4882.

[18] C. Combet, C. Blanchet, C. Geourjon, G. Deléage, NPS@: network protein sequence analysis, Trends Biochem. Sci. 25 (2000) 147–150.

[19] T. Iwamura, M. Yoneyama, K. Yamaguchi, W. Suhara, W. Mori, K. Shiota, Y. Okabe, H. Namiki, T. Fujita, Induction of IRF-3/-7 kinase and NF-kappaB in response to double-stranded RNA and virus infection: common and unique pathways, Genes Cells 6 (2001) 375–388.

[20] H. Kato, S. Sato, M. Yoneyama, M. Yamamoto, S. Uematsu, K. Matsui, T. Tsujimura, K. Takeda, T. Fujita, O. Takeuchi, S. Akira, Cell type-specific involvement of RIG-I in antiviral response, Immunity 23 (2005) 19–28.

[21] M. Gack, Y. Shin, C. Joo, T. Urano, C. Liang, L. Sun, O. Takeuchi, S. Akira, Z. Chen, S. Inoue, J. Jung, TRIM25 RING-finger E3 ubiquitin ligase is essential for RIG-I-mediated antiviral activity, Nature 446 (2007) 916–920.

[22] T. Shigemoto, M. Kageyama, R. Hirai, J. Zheng, M. Yoneyama, T. Fujita, Identification of loss of function mutations in human genes encoding RIG-I and mda5: Implications for resistance to type I diabetes, J. Biol. Chem. (2009).

[23] H. Oshiumi, M. Miyashita, N. Inoue, M. Okabe, M. Matsumoto, T. Seya, The ubiquitin ligase Riplet is essential for RIG-I-dependent innate immune responses to RNA virus infection, Cell Host Microbe 8 (2010) 496–509.

Please cite this article in press as: M. Kageyama et al., 55 Amino acid linker between helicase and carboxyl terminal domains of RIG-I functions as a critical repression domain and determines inter-domain conformation, Biochem. Biophys. Res. Commun. (2011), doi:10.1016/j.bbrc.2011.10.015

THE JOURNAL OF BIOLOGICAL CHEMISTRY VOL. 286, NO. 29, pp. 26210–26219, July 22, 2011

Retinoic Acid-inducible Gene I-inducible miR-23b Inhibits Infections by Minor Group Rhinoviruses through Down-regulation of the Very Low Density Lipoprotein Receptor*[S]

Received for publication, February 10, 2011, and in revised form, June 2, 2011 Published, JBC Papers in Press, June 3, 2011, DOI 10.1074/jbc.M111.229856

Ryota Ouda[‡§], Koji Onomoto[‡], Kiyohiro Takahasi[‡¶], Michael R. Edwards[‖‡‡], Hiroki Kato[‡], Mitsutoshi Yoneyama[§§¶¶], and Takashi Fujita[‡§1]**

*From the [‡]Laboratory of Molecular Genetics, Institute for Virus Research, and the [§]Laboratory of Molecular Cell Biology, Graduate School of Biostudies, Kyoto University, Kyoto 606-8507, Japan, the [¶]Institute for Innovative NanoBio Drug Discovery and Development, Graduate School of Pharmaceutical Science, Kyoto University, Kyoto 606-8501, Japan, the [§§]Medical Mycology Research Center, Chiba University, Chiba 260-8673, Japan, the [¶¶]PRESTO Japan Science and Technology Agency, Saitama 332-0012, Japan, the [‖]Department of Respiratory Medicine, National Heart and Lung Institute, Imperial College London, London SW7 2AZ, United Kingdom, the **MRC and Asthma UK Centre in Allergic Mechanisms of Asthma, London SE1 9RT, United Kingdom, and the [‡‡]Centre for Respiratory Infection, London SW7 2AZ, United Kingdom*

In mammals, viral infections are detected by innate immune receptors, including Toll-like receptor and retinoic acid inducible gene I (RIG-I)-like receptor (RLR), which activate the type I interferon (IFN) system. IFN essentially activates genes encoding antiviral proteins that inhibit various steps of viral replication as well as facilitate the subsequent activation of acquired immune responses. In this study, we investigated the expression of non-coding RNA upon viral infection or RLR activation. Using a microarray, we identified several microRNAs (miRNA) specifically induced to express by RLR signaling. As suggested by Bioinformatics (miRBase Target Data base), one of the RLR-inducible miRNAs, miR-23b, actually knocked down the expression of very low density lipoprotein receptor (VLDLR) and LDLR-related protein 5 (LRP5). Transfection of miR-23b specifically inhibited infection of rhinovirus 1B (RV1B), which utilizes the low density lipoprotein receptor (LDLR) family for viral entry. Conversely, introduction of anti-miRNA-23b enhanced the viral yield. Knockdown experiments using small interfering RNA (siRNA) revealed that VLDLR, but not LRP5, is critical for an efficient infection by RV1B. Furthermore, experiments with the transfection of infectious viral RNA revealed that miR-23b did not affect post-entry viral replication. Our results strongly suggest that RIG-I signaling results in the inhibitions of infections of RV1B through the miR-23b-mediated down-regulation of its receptor VLDLR.

Among the viral components that trigger the antiviral responses of a host, nucleic acids have been considered critical. In invertebrates and plants, the RNA interference (RNAi) system, which destroys non-self RNA in a sequence-dependent manner, is the major antiviral mechanism (1–3). In mammals, certain RNA structures rather than primary sequences are sensed as non-self to initiate a series of antiviral programs including the activation of type I IFN genes. There are at least two receptor systems functioning as sensors to detect viral RNA signatures: the endosomal Toll-like receptor (TLR)[2] 3 and TLR7/8, which interact with extracellular viral RNA (4), and the cytosolic RIG-I, melanoma differentiation associated gene 5 and laboratory of genetics and physiology 2, collectively termed the RLR (5, 6), which sense intracellular viral RNA with a double-stranded and/or 5′-triphosphate structure (7). Signaling generated by the innate immune receptors is transduced through networks with various adaptor molecules and results in the activation of IFN genes (8–10). IFN is secreted, thus expanding the antiviral signal to other cells through physical interaction with cell surface receptors thereby activating the IFN-stimulated genes (ISGs) (11). Several ISGs execute antiviral activity by inhibiting viral transcription, translation, viral assembly, and release of viral particles from the cells. Another feature of the IFN system is that it is tightly regulated by positive and negative feedback loops (12).

Although the RNAi system is operative in mammals, the IFN system appears to dominate the antiviral immune response. Recently, non-coding RNA known as miRNA has received much attention for its post-transcriptional regulation of gene expression (13, 14). Over 500 miRNA-encoding genes, which are exclusively transcribed by RNA polymerase II, have been identified in mammals. These primary miRNAs are processed by the enzyme Drosha into hairpin loop-containing pre-miRNAs, which are then subjected to export from the nucleus to cytoplasm via exportin 5 (15). Further enzymatic processing of the pre-miRNAs by Dicer leads to generation of a mature

* This work was supported in part by a Grant-in-aid from the Ministry of Education, Science, Sports and Culture in Japan, the Ministry of Health, Labor, and Welfare, the PRESTO Japan Science and Technology Agency, the Uehara Memorial Foundation, the Mochida Memorial Foundation for Medical and Pharmaceutical Research, and Nippon Boehringer Ingelheim.

[S] The on-line version of this article (available at http://www.jbc.org) contains supplemental Figs. S1–S4.

[1] To whom correspondence should be addressed: Laboratory of Molecular Genetics, Institute for Virus Research, Kyoto University, Kyoto 606-8507, Japan. Tel./Fax: 81-75-751-4031; E-mail: tfujita@virus.kyoto-u.ac.jp.

[2] The abbreviations used are: TLR, Toll-like receptor; RIG-I, retinoic acid-inducible gene I; LGP2, laboratory of genetics and physiology 2; VLDLR, very low density lipoprotein receptor; LRP, LDLR-related protein; SeV, Sendai virus; NDV, Newcastle disease virus; VSV, vesicular stomatitis virus; EMCV, encephalomyocarditis virus; RV, rhinovirus; ISG, IFN-stimulated gene; CARD, caspase recruitment domain; IRF, IFN regulatory factor; NP, nucleocapsid protein; ICAM-1, intercellular adhesion molecule 1.

miRNA duplex that is loaded into the RNA-induced silencing complex, which is then guided by the miRNA to complementary messenger RNAs. Notably, the sequence complementary in the 6–8-base pair "seed region" at the 5′ end of the miRNA seems to determine the specificity of miRNA-target mRNA interaction (16, 17).

Accumulated information has revealed that some miRNAs are involved in immune regulation. Expression profiling showed that stimulation of monocytes with lipopolysaccharide (LPS) induced the expression of miR-146. miR-146 targets tumor necrosis factor receptor-associated factor 6 (*Traf6*) and interleukin-1 receptor-associated kinase 1(*Irak1*), encoding components of the TLR signaling pathway, suggesting a negative feedback loop (18). Furthermore, liver-specific miR-122 contributes to the liver tropism of the hepatitis C virus by accelerating the binding of ribosomes to the viral RNA and hence aiding translation (19–21). These reports highlight the importance of understanding the function of miRNAs.

In this report, we examined miRNA expression upon RIG-I signaling and identified 37 miRNAs. Among them, miR-23b exhibited antiviral activity to rhinovirus (RV) 1B. RV, a member of the family *Picornaviridae*, causes an extensive range of human respiratory disorders including the common cold, viral bronchiolitis, and exacerbations of asthma and chronic obstructive pulmonary disease (22–26). Recently, primary human bronchial epithelial cells from asthmatics were found to be defective in IFN-β and IFN-λ mRNA and protein, (27, 28), providing a likely explanation for the increased vulnerability to virus-induced asthma exacerbations. Furthermore, it was revealed that TLR3, RIG-I, and melanoma differentiation associated gene 5 were important for RV-inducing innate responses (29–31). Our analyses revealed that miR-23b blocks infections of RV1B through down-regulation of its receptor, VLDLR. This is a novel antiviral mechanism activated by RIG-I signaling.

EXPERIMENTAL PROCEDURES

Cell Culture—HeLa cells were maintained in Dulbecco's modified Eagle's medium with fetal bovine serum and penicillin-streptomycin (100 units/ml and 100 μg/ml, respectively). L929 cells were maintained in minimum essential medium with fetal bovine serum and penicillin-streptomycin (50 units/ml and 100 μg/ml, respectively).

miRNA Microarray—Total RNA was isolated using TRIzol (Invitrogen) and miRNA was purified with a PureLink miRNA Isolation Kit (Invitrogen). The purified miRNA was labeled using Label IT miRNA Labeling Kits (Mirus). Hybridization was performed, using a three-dimensional gene miRNA Oligo Chip (TORAY).

Viral Infection—Cells were treated with the culture medium ("mock-treated") or infected with SeV, NDV, VSV, EMCV, RV16, or RV1B in serum-free and antibiotic-free medium. After adsorption for 1 h at 37 °C, the medium was changed and infection was continued for 24 h in the presence of serum-containing DMEM.

Treatment with Interferon-β (IFN-β)—HeLa cells were maintained in 12-well plates in the presence of serum-containing DMEM. Recombinant human IFN-β (1000 units/ml) was added to each well.

Plaque Assay—L929 cells were seeded in 24-well plates (2.5×10^5 cells/well) in minimal essential medium with 5% FBS for 24 h at 37 °C. After cell propagation, the growth medium was removed and serial dilutions of viral supernatants in serum-free and antibiotic-free minimal essential medium were added to the wells. The inoculated cells were further incubated to allow adsorption of the virus for 1 h at 37 °C. Subsequently, a mixture of agar overlay was added and the plates were incubated at 37 °C for 24 h. The plaques were visualized by staining with a 0.02% neutral red solution. The viral titer is expressed as plaque forming units.

Transfection of miR-23b and Anti-miR-23b—Double-stranded RNA oligonucleotides representing mature sequences that mimic endogenous miR-23b and anti-miR-23b (Ambion) were transfected into HeLa cells with RNAi MAX (Invitrogen) according to the manufacturer's instructions. Silencer negative control #2 small interfering RNA (Ambion) at the same concentration as miR-23b and anti-miR-23b was used in each experiment.

Real-time PCR—Total RNA was isolated using TRIzol (Invitrogen). Real-time PCR for miR-23b, -24, and -27b was performed using the TaqMan MicroRNA Reverse Transcription Kit (Applied Biosystems) according to the manufacturer's protocol. Normalization was performed by using RNU48 primers and probes. Real-time PCR was performed using TaqMan Gene Expression Assay probes for IFN-β and IL-6. The 18S rRNA gene was used as an internal control to normalize differences in each sample. The expression levels for each gene were assessed relative to the expression of 18S rRNA. Real-time PCR for RV RNA was performed using the following primers and probe: RV forward, 5-GTGAAGAGCCSCRTGTGCT-3, RV reverse, 5-GCTSCAGGGTTAAGGTTAGCC-3, RV probe, 5-TGAGTC-CTCCGGCCCCTGAATG-3.

Amido Black Staining—Cells were washed in PBS three times and fixed with methanol. 0.5% Amido Black solution was added and incubated 20 min at RT. After 20 min, the Amido Black solution was removed and eluted by 0.1 M NaOH. 630 nm absorption was measured.

$TCID_{50}$—The RV1B titer was measured by the Reed-Muench method (43).

Small Interfering RNA (siRNA) Knockdown of VLDLR and LRP5—siRNA for VLDLR (Digital Biology) and siRNA for LRP5 (IDT) were transfected into HeLa cells with RNAi MAX (Invitrogen) according to the manufacturer's instructions. Negative control siRNA (Digital Biology) at the same concentration as siVLDLR and siLRP5 was used in each experiment.

Immunoblotting—Cells were lysed with Nonidet P-40 lysis buffer (50 mM Tris (pH 8), 150 mM NaCl, and 1% Nonidet P-40). The lysate was resolved by SDS-PAGE (30 μg of protein/lane). Proteins were transferred to a nitrocellulose membrane. The membrane was blocked in 5% milk for 30 min at room temperature and probed with mouse anti-SeV Nucleocapsid protein, mouse anti-NDV Nucleocapsid protein, mouse anti-VLDLR (Santa Cruz sc-18824), or rabbit anti-LRP5 (Cell Signaling D23F7). Ab binding was detected with alkaline phosphatase-conjugated anti-mouse or anti-rabbit IgG.

RV Genomic RNA Isolation and Transfection—RV-containing medium was centrifuged at 10,000 × *g* for 24 h. The pellet

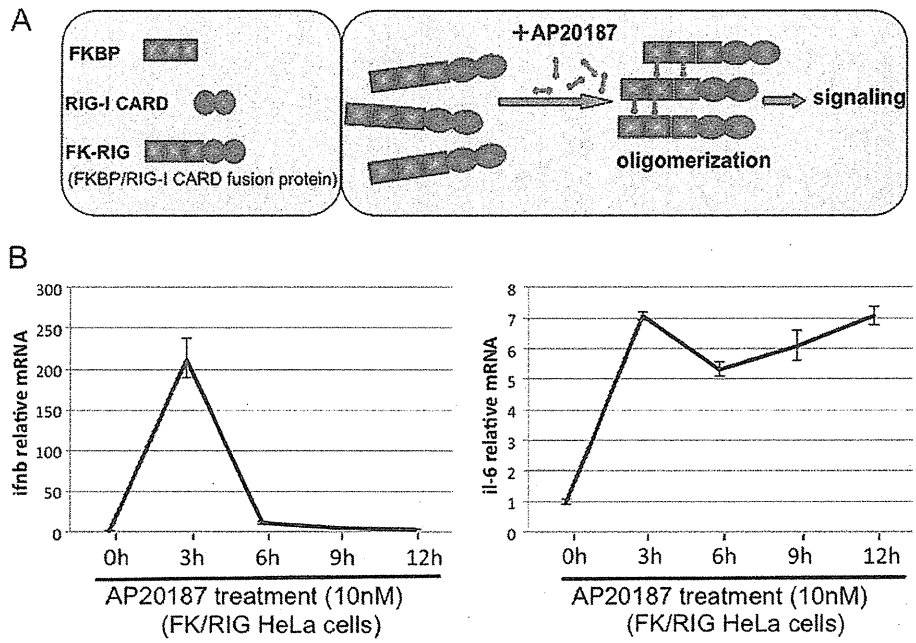

FIGURE 1. **Artificial oligomerization of the CARD of RIG-I results in signaling to activate the IFN-β and IL-6 genes.** *A*, schematic representation of the FK/RIG fusion protein and its oligomerization by a cross-linking reagent, AP20187. *B*, HeLa cells stably expressing FK/RIG were treated with AP for the period indicated and cells were harvested to examine endogenous IFN-β and IL-6 mRNA levels by real-time PCR.

was suspended in TRIzol (Invitrogen). The RV genomic RNA (0.5 μg) and miR-23b were transfected into HeLa cells with Lipofectamine 2000 (Invitrogen).

Statistical Analysis—Statistical analysis were conducted with an unpaired *t* test, with values of $p < 0.05$ considered statistically significant. Each point in a graph represents the mean ± S.E. for at least three independent experiments.

RESULTS

Induction of miRNA Expression by RIG-I Signaling—To directly examine the impact of the activation of RIG-I on the gene expression profile, we developed an artificial RIG-I activation system (details will be reported elsewhere).[3] Briefly, the N-terminal signaling domain of RIG-I, caspase recruitment domain (CARD), was introduced into the ARGENT™ Regulated Homodimerization Kit (ARIAD). The resultant FKBP/RIG-I CARD fusion protein (FK/RIG) allowed CARD to oligomerize by the chemical compound, AP20187 (AP), and to introduce CARD-mediated signaling into the cells (Fig. 1*A*). As shown in Fig. 1*B*, the endogenous mRNA levels of IFN-β and IL-6 in HeLa cells stably expressing FK/RIG (HeLa FK/RIG) were significantly increased by the enforced oligomerization of RIG-I CARD (Fig. 1*B*). Furthermore, microarray analyses of the transcripts of these cells revealed transient expression of IFN genes and ISGs with a concomitant induction of IFN regulatory factor (IRF-3) dimerization and NF-κB DNA-binding activity (data not shown). Thus we concluded that the FK/RIG system could mimic the virus-induced activation of RIG-I signaling.

To analyze the miRNA expression profile in HeLaFK/RIG cells, RNA fractions were prepared at 3, 6, 9, and 12 h after the addition of AP and subjected to analysis with a miRNA

[3] K. Onomoto, M. Yoneyama, and T. Fujita, unpublished data.

TABLE 1
miRNA induced by RIG-I-mediated signaling

HeLa cells stably expressing FK/RIG were treated with AP for the periods indicated and miRNA expression was determined by miRNA microarray (*TORAY*). The relative expression (fold-increase compared to the baseline miRNA level at 0 h) of representative miRNA whose expression was up-regulated more than 2-fold is shown. The opposite strand of miRNA is denoted with an asterisk (*).

	AP20187 treatment (FK/RIG-HeLa cells)				
	0 h	3 h	6 h	9 h	12 h
miR-423–3p	1.00	2.31	2.77	4.34	4.59
miR-301b	1.00	2.31	UD[a]	UD	UD
miR-923	1.00	3.63	1.34	1.50	0.84
miR-181a*	1.00	UD	7.16	UD	UD
miR-23b	1.00	1.47	2.32	1.03	1.27
miR-125b	1.00	1.94	2.73	1.16	1.38
miR-505*	1.00	UD	2.41	UD	UD
miR-940	1.00	UD	2.11	UD	UD
miR-1226	1.00	0.90	2.05	UD	UD
miR-1229	1.00	UD	2.80	UD	UD
miR-1281	1.00	UD	2.21	UD	UD
miR-149	1.00	UD	0.99	3.36	UD
miR-188–5p	1.00	1.85	1.36	3.70	UD
miR-320	1.00	1.22	1.31	2.62	1.71
miR-200c	1.00	1.20	1.03	2.63	UD
miR-362–5p	1.00	1.09	0.94	5.65	UD
miR-425*	1.00	UD	UD	8.81	UD
miR-769–3p	1.00	1.00	1.01	2.65	UD
miR-801	1.00	1.09	0.92	9.18	1.27
miR-29b-1*	1.00	1.43	1.27	2.00	UD
miR-92b*	1.00	0.70	0.88	2.29	UD
miR-1225–3p	1.00	UD	UD	7.16	UD
miR-1228	1.00	UD	1.24	5.77	UD
miR-1249	1.00	UD	UD	5.89	UD
miR-1280	1.00	0.63	1.19	8.00	1.74
miR-664	1.00	1.55	UD	23.75	UD
miR-664*	1.00	1.55	UD	22.62	UD
miR-19b	1.00	1.26	1.40	1.14	2.05
miR-7i	1.00	1.42	1.50	1.68	2.92
miR-484	1.00	0.84	1.38	1.67	2.04
miR-500*	1.00	1.58	1.76	1.73	3.18
miR-421	1.00	1.61	1.90	0.96	2.11
miR-671–5p	1.00	UD	UD	UD	5.38
miR-768–5p	1.00	0.61	0.57	UD	2.94
miR-939	1.00	0.79	0.71	UD	2.75
miR-320b	1.00	1.39	1.44	1.92	2.20
miR-1304	1.00	1.69	1.9	UD	31.12

[a] UD, undetermined.

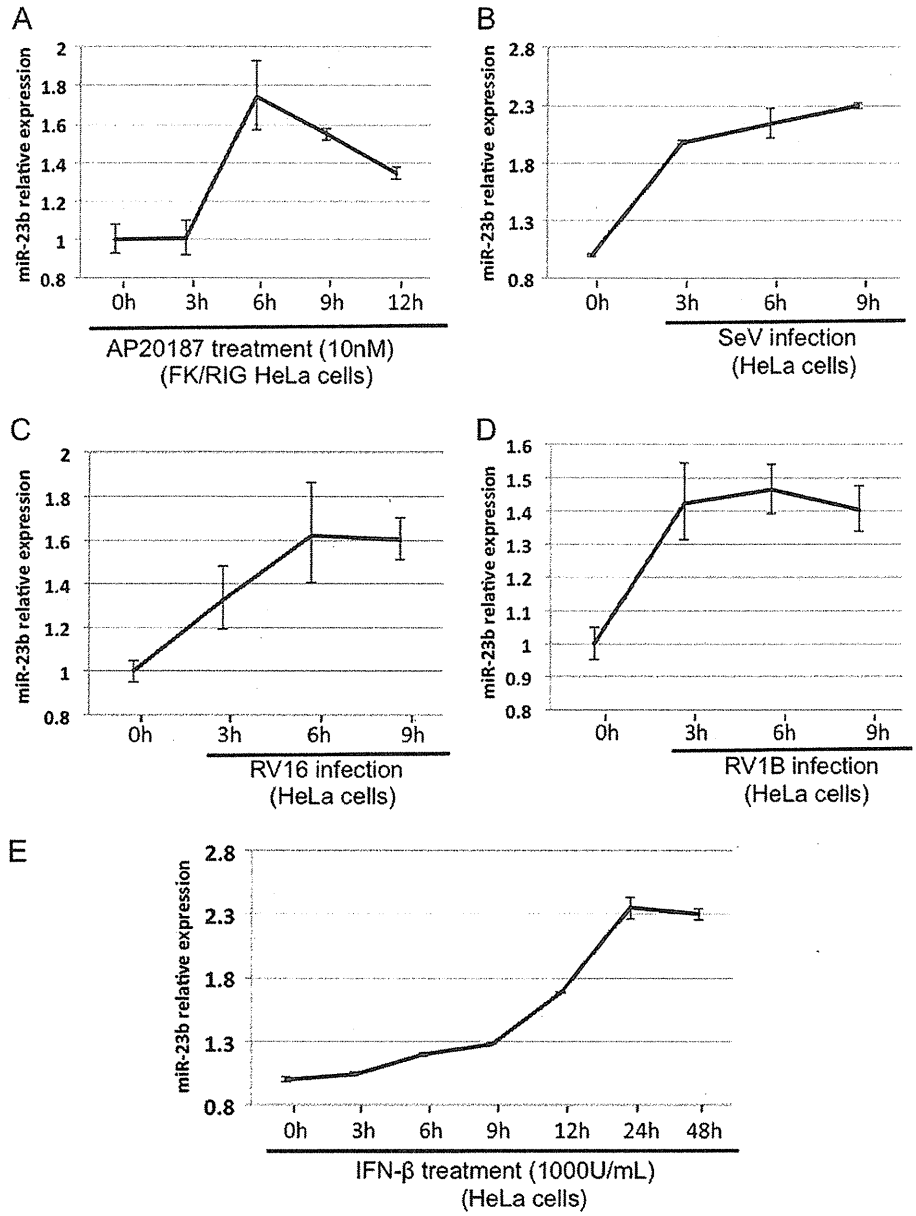

FIGURE 2. **Induction of miR-23b by RIG-I signaling, SeV and RV infection, or IFN-β treatment.** HeLa cells stably expressing FK/RIG were treated with AP (*A*). *B–E*, HeLa cells were infected with SeV (*B*), infected with RV16 (*C*), RV1B (*D*), or treated with IFN-β (1000 units/ml) (*E*). The miRNA fraction was extracted at the time points indicated and the amount of miR-23b was determined by real-time PCR.

microarray (TORAY) that covers 900 miRNAs. The expression level of several miRNAs was up- or down-regulated after the addition of AP (supplemental Fig. S1), the miRNAs exhibiting elevated levels of expression are listed in Table 1. For up-regulated miRNA, the induction kinetics appear to be different. This is commonly observed for different ISGs, presumably the induction is regulated by transcription and post-transcriptional mechanisms. Certainly this issue requires further investigation. Among these RIG-I-inducible miRNA, we focused on miR-23b because (i) it has been reported that miR-23b is regulated by NF-κB (32) and (ii) a data base search revealed that miR-23b has several target sites on mRNA encoding VLDLR (see below). To confirm the results obtained with the miRNA microarray, we monitored expression of miR-23b by real-time PCR. AP treatment resulted in a 1.7-fold increase in miR-23b at 6 h in HeLaFK/RIG with similar kinetics as in the microarray assay (Fig. 2*A*). The Sendai virus (SeV) and two strains of rhinovirus (RV16 and RV1B) also induced miR-23b accumulation (Fig. 2, *B–D*) with similar kinetics to the endogenous IFN-β mRNA expression (supplemental Fig. S2, *A–C*). miR-23b is reported to be derived from the polycistronic miRNA cluster that consists of miR-23b-27b-24 in the human gene, *C9orf3* (supplemental Fig. S3*A*) (32). As expected, the expression of miR-24 and miR-27b was also induced by RV16 and RV1B infection (supplemental Fig. S3, *B* and *C*), suggesting that these miRNA are regulated by a common mechanism. On the other hand, treatment of cells

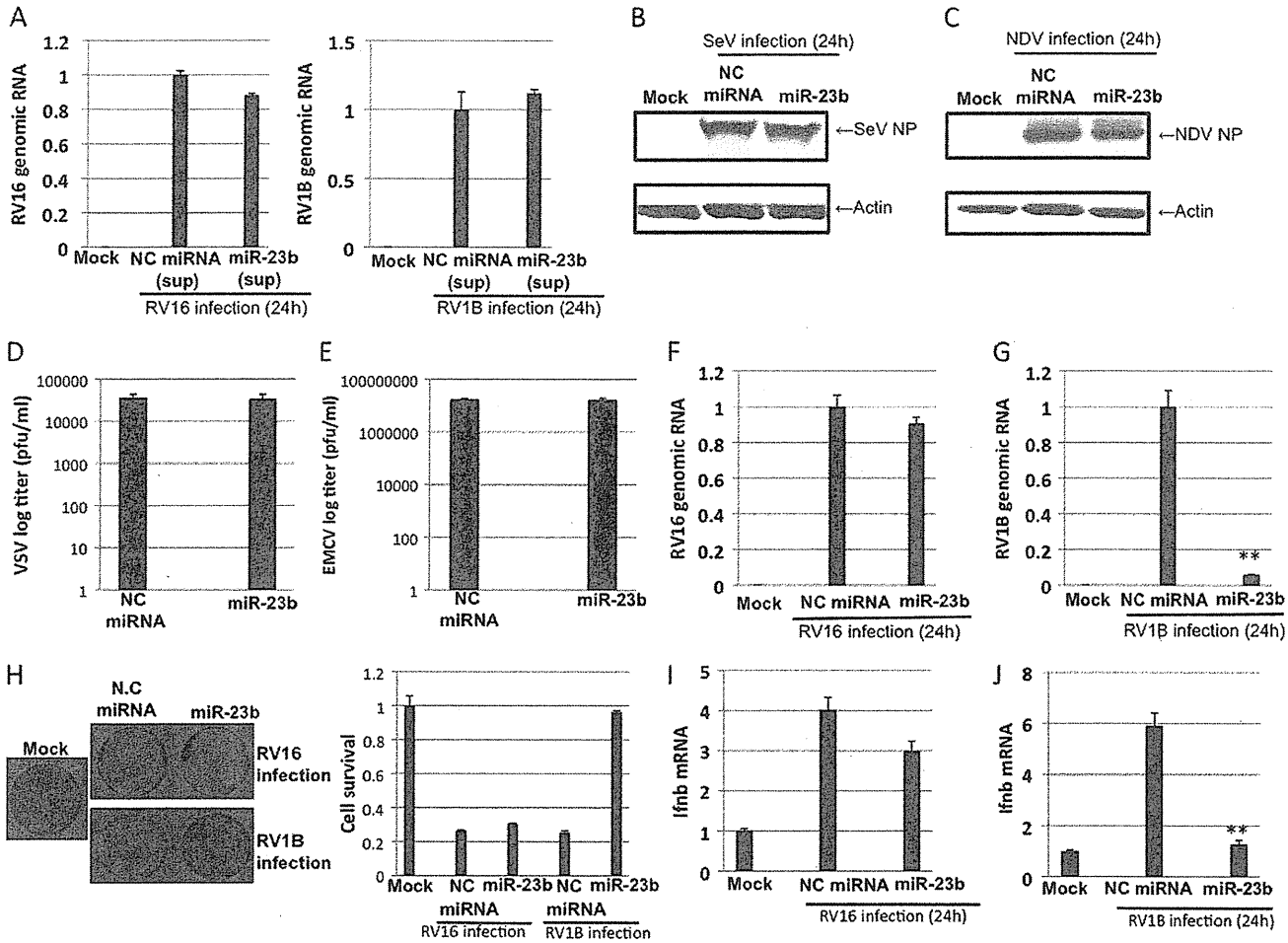

FIGURE 3. **The effect of miR-23b transfection on viral growth.** *A*, HeLa cells were transfected with negative control miRNA (*NC miRNA*) or miR-23b for 48 h, the culture supernatant (*sup*) was collected, and HeLa cells were treated with supernatant for 24 h and then infected with RV for 24 h. Levels of RV genomic RNA were determined by real-time PCR. *B-G*, HeLa cells transfected with NC miRNA or miR-23b for 48 h were infected with SeV (*B*), NDV (*C*), VSV (*D*), EMCV (*E*), RV16 (*F*), or RV1B (*G*) for an additional 24 h. The viral NP level was determined by Western blotting (*B*, SeV; *C*, NDV). Infectivity in the culture supernatant was determined by plaque assay (*D*, VSV; *E*, EMCV). Levels of RV genomic RNA were determined by real-time PCR (*F*, RV16; *G*, RV1B) using specific primer sets. *H*, Amido Black staining of miRNA-transfected and RV-infected cells. IFN-β mRNA levels of the RNA samples in *F* and *G* are shown in *I* and *J*, respectively. **, $p < 0.005$.

with IFN-β also induced miR-23b expression with a peak at 24 h, suggesting that in addition to RIG-I-mediated signaling, IFN receptor-mediated signaling induces miR-23b expression albeit with slow kinetics (Fig. 2*E*). These results suggest that, although the expression of miR-23b is up-regulated by both RIG-I- and IFN-mediated signaling, the former is mainly responsible for transient induction after oligomerization of RIG-I CARD.

Selective Effect of miR-23b on Rhinovirus 1B Replication—To examine whether miR-23b has an antiviral effect, HeLa cells were transiently transfected with synthetic miR-23b (Ambion), which is a chemically modified double-stranded RNA and mimics endogenous miR-23b, or control miRNA (NC miRNA) for 48 h and infected with SeV, Newcastle disease virus (NDV), vesicular stomatitis virus (VSV), encephalomyocarditis virus (EMCV), and two strains of rhinovirus (RV16 and RV1B) for 24 h. RV16 and RV1B are representative of major and minor group RVs, respectively, and utilize distinct cellular receptors for viral entry (33–35). First, to exclude the possibility that miRNA induces production of antiviral humoral factors such as IFNs, we examined antiviral activity in the culture supernatant of HeLa cells transfected with either control miRNA or miR23b. The supernatant did not affect viral RNA yields from RV-infected HeLa cells, indicating that miR23b does not induce production of antiviral cytokines (Fig. 3*A*). Next, we tried to examine the effect of miR-23b on viral growth. For SeV and NDV infections, nucleocapsid proteins (NPs), which are known to interact with viral genome in infected cells, were detected by Western blotting with specific antibodies (Fig. 3, *B and C*). Transfection with miR-23b did not influence the accumulation of NPs in SeV- or NDV-infected cells, suggesting no effect on growth of these viruses. In the case of VSV and EMCV, we determined viral titer from the infected cells by plaque assays (Fig. 3, *D* and *E*). Transfection with miR-23b did not influence yields of VSV or EMCV. For RV16 and RV1B, the accumulation of viral RNA was examined by real-time PCR. The introduction of miR-23b moderately reduced the amount of RV16 RNA, however, a dramatic

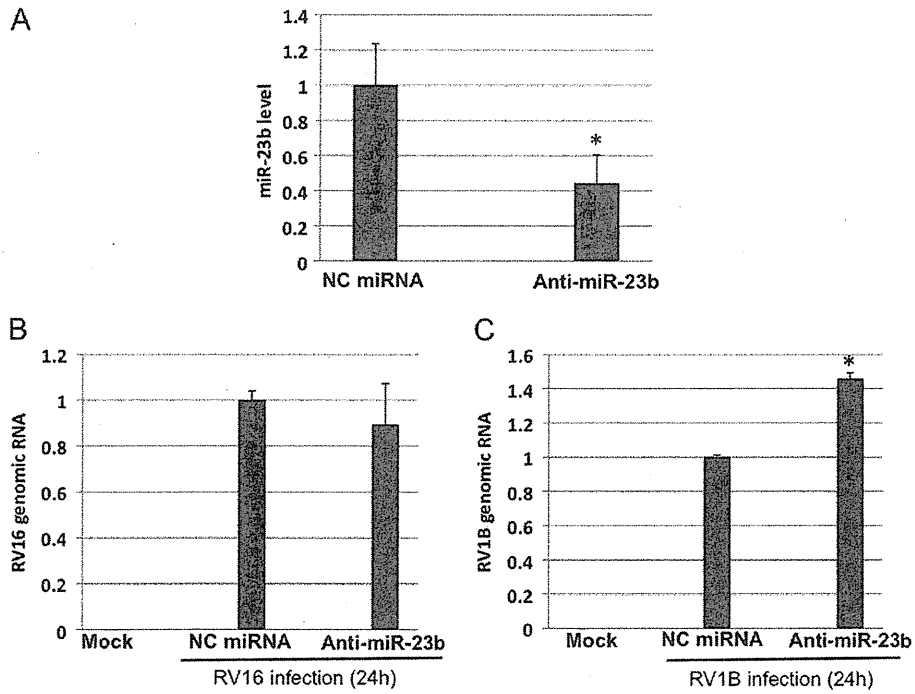

FIGURE 4. **Anti-miR-23b enhanced RNA yields of RV1B.** HeLa cells were transfected with NC miRNA or anti-miR-23b for 48 h and infected with RV for 24 h. *A*, the expression of miR-23b after anti-miR-23b transfection was determined by real-time PCR. *B* and *C*, the yield of genomic RNA of RV16 (*B*) and RV1B (*C*) was determined by real-time PCR. *, $p < 0.05$.

reduction of RV1B viral RNA was observed (Fig. 3, *F* and *G*). Furthermore, RV1B titer was severely reduced by miR-23b treatment (supplemental Fig. S4*A*). Consistent with this, the cell survival rate was significantly restored by miR-23b transfection after RV1B infection but not RV16 infection (Fig. 3*H*). Again, to verify whether the effect of miR-23b on viral RNA yield of RV1B is indirectly mediated by the secreted IFNs, endogenous IFN-β mRNA levels in miR-23b-transfected and RV-infected cells were determined (Fig. 3, *I* and *J*). In cells infected with RV16 or RV1B, IFN-β mRNA levels were closely correlated to the viral yields (compare Fig. 3, *F* and *G* to *I* and *J*, respectively), suggesting that the decrease of RV1B RNA caused by miR-23b is unlikely due to enhanced production of IFN-β. Taken together, these results suggest that miR-23b has an antiviral effect specific to RV1B.

Down-regulation of miR-23b Expression Resulted in Increased RNA Yields of RV1B—To further investigate the mechanism of the antiviral effect of miR-23b on RV1B, we transiently expressed anti-miR-23b in HeLa cells. This anti-miR-23b (Ambion) is a chemically modified single-stranded RNA and specifically bind miR-23b, inhibiting the function of miR-23b. The transfection led to a 60% decrease of endogenous miR-23b production, compared with NC-miRNA transfection (Fig. 4*A*). Under these conditions, the RV16 RNA level was not changed by anti-miR-23b (Fig. 4*B*). On the other hand, the RV1B RNA level was significantly increased by anti-miR-23b (Fig. 4*C*). Consistent with this, RV1B titer was clearly increased by anti-miR-23b transfection (supplemental Fig. S4*B*). These results further confirm that the inhibition of RV1B RNA is mediated by miR-23b.

LRP5 and VLDLR Are Targets of miR-23b—A bioinformatic-based (microRNA.org) search of databases revealed 1 and 6 target sites on mRNA encoding LDLR-related protein 5 (LRP5) and VLDLR, respectively (Fig. 5, *A* and *B*). Because it has been reported that minor group RVs, including RV1B, use LDLR family proteins (LDLR, VLDLR, and LRPs) as cellular receptors and major group RVs utilize ICAM-1, we speculate that miR-23b specifically affects expression of RV1B receptors. To confirm this, miR-23b was introduced into HeLa cells and its effect on expression of LRP5 and VLDLR was determined by Western blotting (Fig. 5). The levels of LRP5 and VLDLR were significantly reduced by transfection of miR-23b, suggesting that miR-23b targets mRNA for these proteins. Furthermore, induction of endogenous miR-23b expression through the activation of FK/RIG by AP treatment in HeLaFK/RIG cells resulted in decreased levels of LRP5 and VLDLR (Fig. 5*C*). However, anti-miR-23b blocked this reduction. These results strongly suggest that endogenous miR-23b participate in the down-regulation of LRP5 and VLDLR expression via RIG-I-mediated signaling.

Knockdown of VLDLR Reduced RV1B RNA Yields—To clarify which of the miR-23b-targeted LDLR family proteins are critical for RV1B infections, we individually knocked down LRP5 and VLDLR using specific siRNA (Fig. 6*A*) and the RV viral RNA yield was compared (Fig. 6, *B* and *C*). As expected, the viral RNA of RV16, which utilizes ICAM-1 as a receptor (36), was not affected by either siRNA treatment. However, knockdown of VLDLR dramatically reduced RV1B RNA yields. Knockdown of LRP5 enhanced RV1B RNA yields, however, this effect was not observed in cells with the double

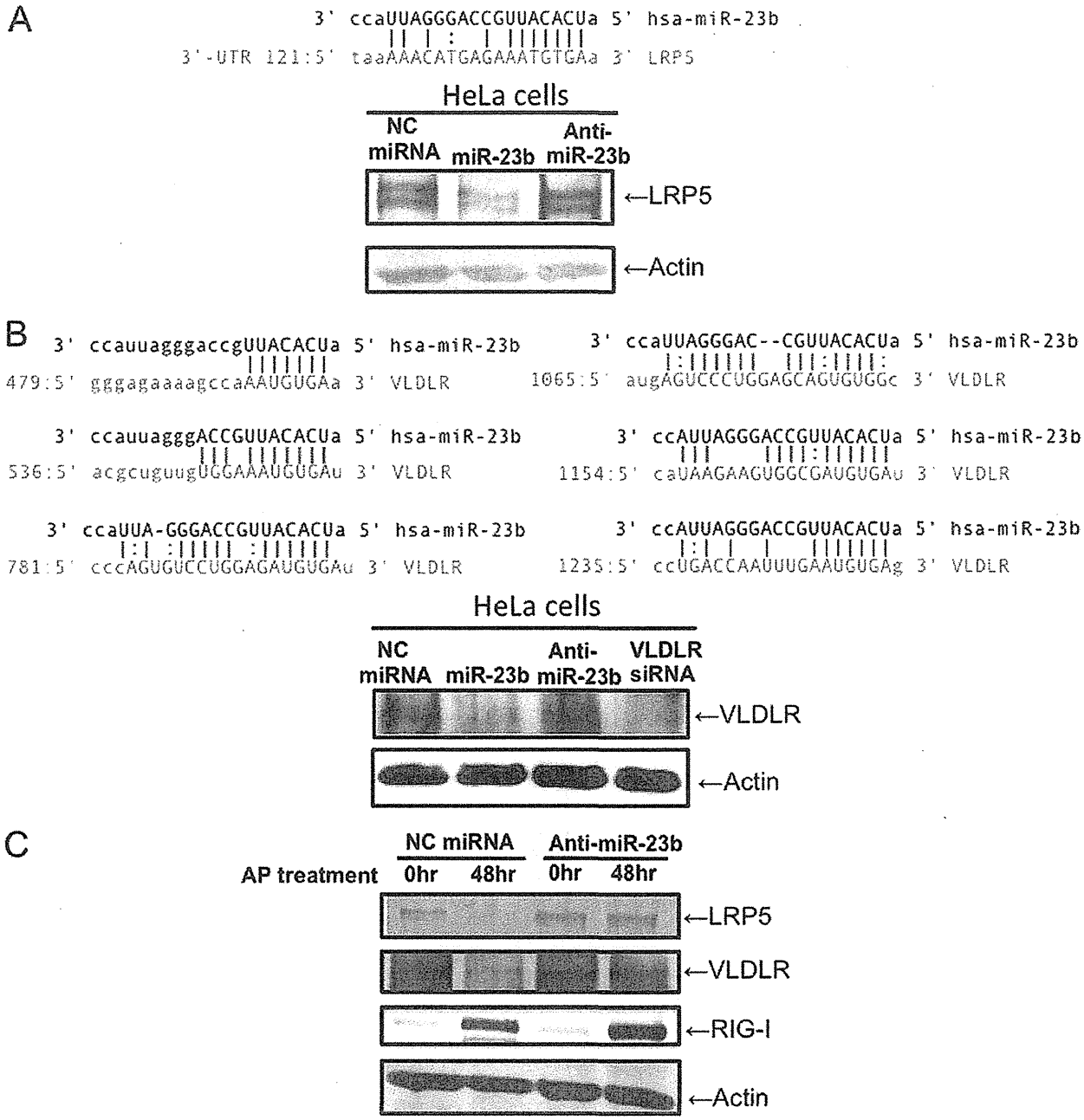

FIGURE 5. **miR-23b targets LRP5 and VLDLR.** *A* and *B*, the results of the search for target sequences of miR-23b (miRBase Target Data base). Candidate sequences in LRP5 (*A*) and VLDLR (*B*) mRNA are shown. HeLa cells were transfected with NC miRNA, miR-23b, or anti-miR-23b for 48 h and LRP5 (*A*) and VLDLR (*B*) were detected by Western blotting. *C*, HeLa FK/RIG cells were transfected with either NC miRNA or anti-miR-23b for 24 h and AP20187 was treated for 48 h. LRP5 and VLDLR were detected by Western blotting.

knockdown of VLDLR and LRP5. The protein level of VLDLR is slightly increased in cells transfected with LRP5 siRNA by an unknown mechanism (Fig. 6*A*). The higher RV1B replication in cells transfected with LRP5 siRNA (Fig. 6*C*) could be explained by the increased expression of its receptor, VLDLR. These results suggest that VLDLR but not LRP5 is critical for viral growth of RV1B.

miR-23b Did Not Influence Intracellular Replication of RV1B—The above results suggest that miR-23b blocks entry of RV1B by inhibiting expression of the receptor VLDLR. Because there are several reports that viral genomic RNA is directly targeted by host miRNA (37, 38), we investigated whether RV1B replication initiated by transfection of infectious viral genomic RNA is affected by miR-23b. HeLa cells were co-transfected with viral RNA and miRNA (Fig. 7), and the cells were harvested to examine the level of miR-23b and viral RNA at 3 and 9 h post-infection. High levels of miR-23b were detected in miR-23b-transfected but not NC miRNA-transfected cells, suggesting that the miR-23b was efficiently incorporated, and remained in the cells at 9 h after transfection (Fig. 7*A*). In the cells transfected with

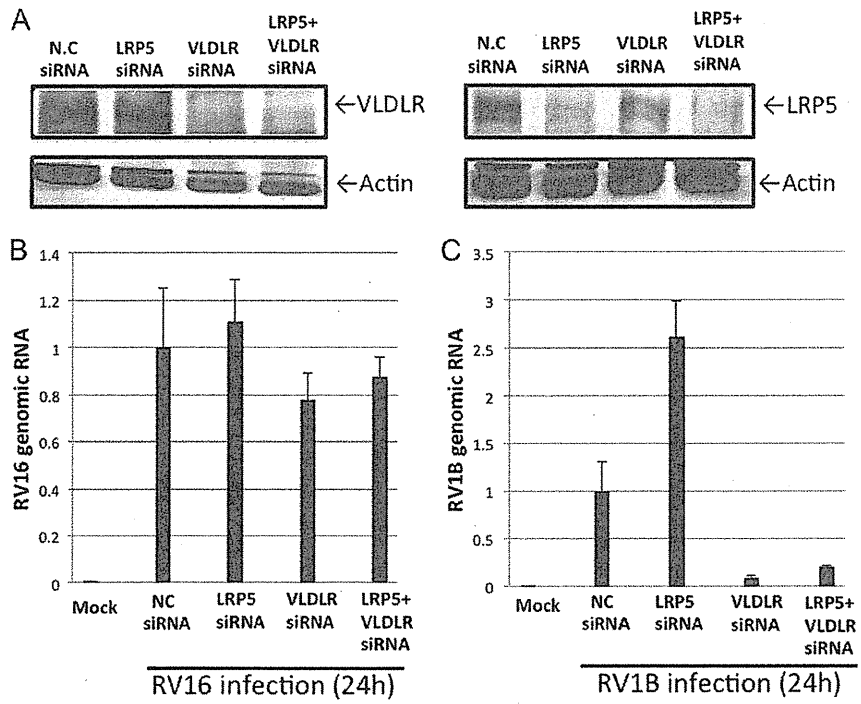

FIGURE 6. **Knockdown of VLDLR blocks accumulation of viral RNA in RV1B-infected cells.** HeLa cells were transfected with control siRNA or siRNA targeting VLDLR or LRP5 as indicated. *A–C*, at 48 h after the transfection, cells were mock infected or infected with RV16 or RV1B for an additional 24 h. VLDLR and LRP5 were detected by Western blotting in mock-infected cells (*A*). RNA levels of RV16 (*B*) or RV1B (*C*) were determined by real-time PCR.

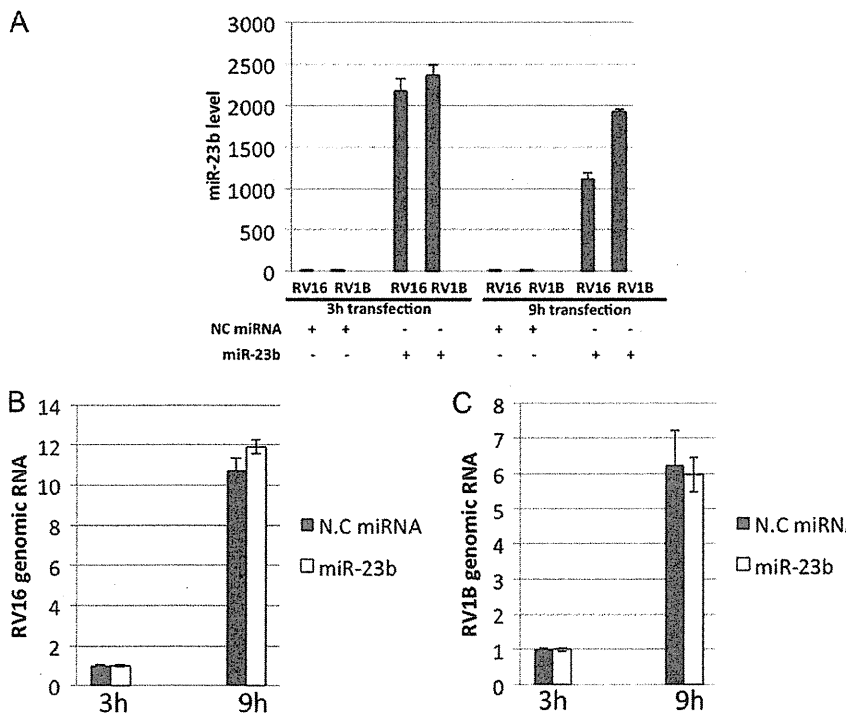

FIGURE 7. **miR-23b did not influence intracellular replication of RV1B.** *A–C*, HeLa cells were co-transfected with RV genomic RNA and NC miRNA or miR-23b for 3 and 9 h. Levels of miR-23b (*A*), RV16 RNA (*B*), and RV1B RNA (*C*) were determined by real-time PCR.

RV16 or RV1B genomic RNAs, although increasing amounts of viral RNAs were detected, no inhibitory effect of miR-23b was observed (Fig. 7, *B* and *C*). These results suggest that miR-23b inhibits infection of RV1B by down-regulating the expression of its major receptor, VLDLR, rather than impairment of the viral replication.

DISCUSSION

It has been well established that IFN treatment activates a Janus kinase-signal transducer activator of transcription (STAT) pathway resulting in activation of a variety of ISGs (39–41). Some ISGs encode proteins, collectively known as antiviral proteins, which directly inhibit viral replication. In this report, we demonstrated an alternative mechanism of inducing an antiviral state, that is, reducing the level of a protein essential for viral infection via activating a gene encoding miRNA. Thus innate immune responses restrict viral replication either by adding antiviral proteins or by removing proteins necessary for viral infection.

In addition to the regulation of host genes, miRNAs targeting viral RNA genomes have been reported. Pedersen and colleagues (38) reported that treatment of hepatic cells with IFN-β resulted in the production of at least eight miRNAs (miR-1, miR-30, miR-128, miR-196, miR-296, miR-351, miR-431, and miR-448) that perfectly complement hepatitis C virus mRNAs. These findings suggest that the mammalian immune system utilizes miRNA to combat viral infections via multiple mechanisms.

We examined 900 miRNAs using a microarray and found that 37 and 28 miRNAs were up- and down-regulated, respectively (Table 1). The results show a marked regulation of miRNA expression upon viral infection (3–4%). In this report, we focused on miR-23b, because its possible target genes encode cell-surface proteins that are known to be viral receptors. Overexpression of miR-23b and anti-miR-23b resulted in repressed and enhanced production of RV1B, respectively. Although miR-23b targets both LRP5 and VLDLR, our analyses revealed the down-regulation of VLDLR to be responsible for the inhibition of RV1B.

Among the minor group rhinovirus there are 12 types of RV (RV1A, RV1B, RV2, RV44, RV47, RV49, RV23, RV25, RV29, RV30, RV31, and RV62). Considering that these minor group RVs commonly utilize VLDLR for their entry, miR-23b should exhibit an antiviral effect on these 12 types RVs. Importantly, the minor group RVs are shown to cause disease more often than the major group RV (42), suggesting that down-regulation of VLDLR by miR-23b is of significance for host defense to the minor group of RVs. Because the binding of viruses to the host cell is the initial step for viral entry, transient down-regulation of cell surface molecules could be an effective strategy to avoid viral transmission.

Artificial activation of RIG-I or infection by SeV and RV resulted in the accumulation of miR-23b with a peak at 6 and 9 h, respectively (Fig. 2). IFN-β treatment also induced the accumulation of miR-23b albeit with slower kinetics and a peak around 24 h. These results suggest that the expression of miR-23b is regulated by similar mechanisms to that of some ISGs, which are stimulated by both IRF-3/IRF-7 and IFN-stimulated gene factor 3 (ISGF3), the trimeric complex of STAT1, STAT2, and IRF-9. As reported previously, NF-κB may participate in the production of miR-23b inducted by viral infection or RIG-I stimulation (32). Because type I IFN is produced and secreted in the initial stages of viral infection, IFN induces the accumulation of miR-23b in uninfected cells, thereby protecting them from initial infection.

In summary, our study presents evidence that RIG-I-mediated signaling up-regulates the expression of 37 miRNAs, one of which, miR-23b, strongly inhibits minor group rhinoviruses through down-regulation of VLDLR, which functions as a receptor for entry into the cell. This finding provides a novel perspective for RIG-I-mediated antiviral effects.

Acknowledgments—We thank Prof. T. Sakaguchi for anti-NDV NP antibody and Prof. K. Atsushi for anti-SeV NP antibody.

REFERENCES

1. Vaucheret, H., Béclin, C., and Fagard, M. (2001) *J. Cell Sci.* **114,** 3083–3091
2. Takaoka, A., and Yanai, H. (2006) *Cell. Microbiol.* **8,** 907–922
3. Baulcombe, D. (2004) *Nature* **431,** 356–363
4. Akira, S., and Takeda, K. (2004) *Nat. Rev. Immunol.* **4,** 499–511
5. Yoneyama, M., Kikuchi, M., Matsumoto, K., Imaizumi, T., Miyagishi, M., Taira, K., Foy, E., Loo, Y. M., Gale, M., Jr., Akira, S., Yonehara, S., Kato, A., and Fujita, T. (2005) *J. Immunol.* **175,** 2851–2858
6. Yoneyama, M., Kikuchi, M., Natsukawa, T., Shinobu, N., Imaizumi, T., Miyagishi, M., Taira, K., Akira, S., and Fujita, T. (2004) *Nat. Immunol.* **5,** 730–737
7. Kato, H., Takeuchi, O., Mikamo-Satoh, E., Hirai, R., Kawai, T., Matsushita, K., Hiiragi, A., Dermody, T. S., Fujita, T., and Akira, S. (2008) *J. Exp. Med.* **205,** 1601–1610
8. Kawai, T., Takahashi, K., Sato, S., Coban, C., Kumar, H., Kato, H., Ishii, K. J., Takeuchi, O., and Akira, S. (2005) *Nat. Immunol.* **6,** 981–988
9. Kumar, H., Kawai, T., Kato, H., Sato, S., Takahashi, K., Coban, C., Yamamoto, M., Uematsu, S., Ishii, K. J., Takeuchi, O., and Akira, S. (2006) *J. Exp. Med.* **203,** 1795–1803
10. Potter, J. A., Randall, R. E., and Taylor, G. L. (2008) *BMC Struct. Biol.* **8,** 11
11. Shingai, M., Ebihara, T., Begum, N. A., Kato, A., Honma, T., Matsumoto, K., Saito, H., Ogura, H., Matsumoto, M., and Seya, T. (2007) *J. Immunol.* **179,** 6123–6133
12. Dalpke, A., Heeg, K., Bartz, H., and Baetz, A. (2008) *Immunobiology* **213,** 225–235
13. Friedman, R. C., Farh, K. K., Burge, C. B., and Bartel, D. P. (2009) *Genome Res.* **19,** 92–105
14. Molnár, A., Schwach, F., Studholme, D. J., Thuenemann, E. C., and Baulcombe, D. C. (2007) *Nature* **447,** 1126–1129
15. Lee, Y., Ahn, C., Han, J., Choi, H., Kim, J., Yim, J., Lee, J., Provost, P., Rådmark, O., Kim, S., and Kim, V. N. (2003) *Nature* **425,** 415–419
16. Gregory, R. I., Chendrimada, T. P., Cooch, N., and Shiekhattar, R. (2005) *Cell* **123,** 631–640
17. Okamura, K., Ishizuka, A., Siomi, H., and Siomi, M. C. (2004) *Genes Dev.* **18,** 1655–1666
18. Taganov, K. D., Boldin, M. P., Chang, K. J., and Baltimore, D. (2006) *Proc. Natl. Acad. Sci. U.S.A.* **103,** 12481–12486
19. Henke, J. I., Goergen, D., Zheng, J., Song, Y., Schüttler, C. G., Fehr, C., Jünemann, C., and Niepmann, M. (2008) *EMBO J.* **27,** 3300–3310
20. Jopling, C. L. (2008) *Biochem. Soc. Trans.* **36,** 1220–1223
21. Sarasin-Filipowicz, M., Krol, J., Markiewicz, I., Heim, M. H., and Filipowicz, W. (2009) *Nat. Med.* **15,** 31–33
22. Vlasak, M., Roivainen, M., Reithmayer, M., Goesler, I., Laine, P., Snyers, L., Hovi, T., and Blaas, D. (2005) *J. Virol.* **79,** 7389–7395
23. Savolainen, C., Blomqvist, S., and Hovi, T. (2003) *Pediatr. Respir. Rev.* **4,** 91–98
24. Message, S. D., Laza-Stanca, V., Mallia, P., Parker, H. L., Zhu, J., Kebadze, T., Contoli, M., Sanderson, G., Kon, O. M., Papi, A., Jeffery, P. K., Stanciu, L. A., and Johnston, S. L. (2008) *Proc. Natl. Acad. Sci. U.S.A.* **105,** 13562–13567
25. Johnston, S. L. (2005) *Proc. Am. Thorac. Soc.* **2,** 150–156
26. Johnston, S. L., Pattemore, P. K., Sanderson, G., Smith, S., Lampe, F., Josephs, L., Symington, P., O'Toole, S., Myint, S. H., Tyrrell, D. A., *et al.*

(1995) *BMJ* **310,** 1225–1229
27. Wark, P. A., Johnston, S. L., Bucchieri, F., Powell, R., Puddicombe, S., Laza-Stanca, V., Holgate, S. T., and Davies, D. E. (2005) *J. Exp. Med.* **201,** 937–947
28. Contoli, M., Message, S. D., Laza-Stanca, V., Edwards, M. R., Wark, P. A., Bartlett, N. W., Kebadze, T., Mallia, P., Stanciu, L. A., Parker, H. L., Slater, L., Lewis-Antes, A., Kon, O. M., Holgate, S. T., Davies, D. E., Kotenko, S. V., Papi, A., and Johnston, S. L. (2006) *Nat. Med.* **12,** 1023–1026
29. Slater, L., Bartlett, N. W., Haas, J. J., Zhu, J., Message, S. D., Walton, R. P., Sykes, A., Dahdaleh, S., Clarke, D. L., Belvisi, M. G., Kon, O. M., Fujita, T., Jeffery, P. K., Johnston, S. L., and Edwards, M. R. (2010) *PLoS Pathog.* **6,** e1001178
30. Hewson, C. A., Jardine, A., Edwards, M. R., Laza-Stanca, V., and Johnston, S. L. (2005) *J. Virol.* **79,** 12273–12279
31. Wang, Q., Nagarkar, D. R., Bowman, E. R., Schneider, D., Gosangi, B., Lei, J., Zhao, Y., McHenry, C. L., Burgens, R. V., Miller, D. J., Sajjan, U., and Hershenson, M. B. (2009) *J. Immunol.* **183,** 6989–6997
32. Zhou, R., Hu, G., Liu, J., Gong, A. Y., Drescher, K. M., and Chen, X. M. (2009) *PLoS Pathog.* **5,** e1000681
33. Marlovits, T. C., Abrahamsberg, C., and Blaas, D. (1998) *J. Virol.* **72,** 10246–10250
34. Nizet, S., Wruss, J., Landstetter, N., Snyers, L., and Blaas, D. (2005) *J. Virol.* **79,** 14730–14736
35. Okun, V. M., Moser, R., Ronacher, B., Kenndler, E., and Blaas, D. (2001) *J. Biol. Chem.* **276,** 1057–1062
36. Grünberg, K., Sharon, R. F., Hiltermann, T. J., Brahim, J. J., Dick, E. C., Sterk, P. J., and Van Krieken, J. H. (2000) *Clin. Exp. Allergy* **30,** 1015–1023
37. Otsuka, M., Jing, Q., Georgel, P., New, L., Chen, J., Mols, J., Kang, Y. J., Jiang, Z., Du, X., Cook, R., Das, S. C., Pattnaik, A. K., Beutler, B., and Han, J. (2007) *Immunity* **27,** 123–134
38. Pedersen, I. M., Cheng, G., Wieland, S., Volinia, S., Croce, C. M., Chisari, F. V., and David, M. (2007) *Nature* **449,** 919–922
39. Wu, A. J., Chen, Z. J., Kan, E. C., and Baum, B. J. (1997) *J. Cell Physiol.* **173,** 110–114
40. Lehtonen, A., Matikainen, S., and Julkunen, I. (1997) *J. Immunol.* **159,** 794–803
41. Meraz, M. A., White, J. M., Sheehan, K. C., Bach, E. A., Rodig, S. J., Dighe, A. S., Kaplan, D. H., Riley, J. K., Greenlund, A. C., Campbell, D., Carver-Moore, K., DuBois, R. N., Clark, R., Aguet, M., and Schreiber, R. D. (1996) *Cell* **84,** 431–442
42. Andries, K., Dewindt, B., Snoeks, J., Wouters, L., Moereels, H., Lewi, P. J., and Janssen, P. A. (1990) *J. Virol.* **64,** 1117–1123
43. Reed, L. J., and Muench, H. (1938) *Am. J. Hygiene* **27,** 493–497

Dysregulation of IFN System Can Lead to Poor Response to Pegylated Interferon and Ribavirin Therapy in Chronic Hepatitis C

Koji Onomoto[1,7¤], Shiho Morimoto[1], Takahisa Kawaguchi[2], Hidenori Toyoda[3], Masami Tanaka[4], Masahiko Kuroda[4], Kazuko Uno[5], Takashi Kumada[3], Fumihiko Matsuda[2], Kunitada Shimotohno[6], Takashi Fujita[1], Yoshiki Murakami[2]*

1 Institute for Viral Research and Graduate School of Bioscience, Kyoto University, Kyoto, Japan, **2** Center for Genomic Medicine, Kyoto University Graduate School of Medicine, Kyoto, Japan, **3** Department of Gastroenterology, Ogaki Municipal Hospital, Ogaki, Japan, **4** Department of Molecular Pathology, Tokyo Medical University, Tokyo, Japan, **5** Louis Pasteur Center for Medical Research, Kyoto, Kyoto, Japan, **6** Research Institute, Chiba Institute for Technology, Narashino, Japan, **7** Research Institute for Science and Engineering, Waseda University, Tokyo, Japan

Abstract

Background: Despite being expensive, the standard combination of pegylated interferon (Peg-IFN)- α and ribavirin used to treat chronic hepatitis C (CH) results in a moderate clearance rate and a plethora of side effects. This makes it necessary to predict patient outcome so as to improve the accuracy of treatment. Although the antiviral mechanism of genetically altered IL28B is unknown, IL28B polymorphism is considered a good predictor of IFN combination treatment outcome.

Methodology: Using microarray, we quantified the expression profile of 237 IFN related genes in 87 CH liver biopsy specimens to clarify the relationship between IFN pathway and viral elimination, and to predict patients' clinical outcome. In 72 out of 87 patients we also analyzed IL28B polymorphism (rs8099917).

Principal Findings: Five IFN related-genes (IFI27, IFI 44, ISG15, MX1, and OAS1) had expression levels significantly higher in nonresponders (NR) than in normal liver (NL) and sustained virological responders (SVR); this high expression was also frequently seen in cases with the minor (TG or GG) IL28B genotype. The expression pattern of 31 IFN related-genes also differed significantly between NR and NL. We predicted drug response in NR with 86.1% accuracy by diagonal linear discriminant analysis (DLDA).

Conclusion: IFN system dysregulation before treatment was associated with poor IFN therapy response. Determining IFN related-gene expression pattern based on patients' response to combination therapy, allowed us to predict drug response with high accuracy. This method can be applied to establishing novel antiviral therapies and strategies for patients using a more individual approach.

Citation: Onomoto K, Morimoto S, Kawaguchi T, Toyoda H, Tanaka M, et al. (2011) Dysregulation of IFN System Can Lead to Poor Response to Pegylated Interferon and Ribavirin Therapy in Chronic Hepatitis C. PLoS ONE 6(5): e19799. doi:10.1371/journal.pone.0019799

Editor: Mathias Lichterfeld, Massachusetts General Hospital, United States of America

Received December 21, 2010; **Accepted** April 11, 2011; **Published** May 13, 2011

Funding: Y.M. was financially supported by the Japanese Ministry of Health, Labour and Welfare. Grants-in-Aid for scientific research were received from the Ministry of Education, Culture, Sports, Science and Technology. The funders had no role in study design, data collection and analysis, decision to publish, or preparation of the manuscript.

Competing Interests: The authors have declared that no competing interests exist.

* E-mail: ymurakami@genome.med.kyoto-u.ac.jp

¤ Current address: Division of Molecular Immunology, Medical Mycology Research Center, Chiba University, Chiba, Japan

Introduction

Hepatitis C virus (HCV) infection affects more than 3% of the world population. Without suitable treatment, chronic hepatitis C (CH) frequently leads to the development of chronic liver diseases such as liver cirrhosis (LC) and hepatocellular carcinoma (HCC) [1]. The current standard treatment for CH is a combination of pegylated-IFN (Peg-IFN)- α and ribavirin (hereafter CH combination therapy). Over a 15-year observation period, the rate of hepatocarcinogenesis was found to be significantly lower in sustained viral responders (SVR) and relapse (R) patients than in non responders (NR) and interferon (IFN) untreated patients [2]. However, CH combination therapy achieves a sustained virological response in 50–55% of patients with HCV genotype 1b infection [3]. Consequently, this creates a pressing need to develop alternative strategies for treating CH.

IFN Type-I and III play various important immunomodulatory roles in both innate immune and acquired immune responses. Four main effector pathways of the IFN-mediated antiviral response have been recognized by gene targeting studies: the Mx GTPase pathway, the 2′, 5′-oligoadenylate-synthetase-directed ribonuclease L (OASL) pathway, the protein kinase R (PKR) pathway and the interferon stimulated gene (ISG) 15 ubiquitin-like pathway. These effector-pathways individually block viral

transcription, degrade viral RNA, inhibit translation and modify protein function to control all steps of viral replication [4–5].

IFN treatment for CH usually results in a high incidence of side effects; therefore, it is important to adjust IFN treatment accurately using a prediction method. Viral factors (HCV genotype, pretreatment viral load, and sequence of HCV gene core and NS5A), [6–7] host factors (obesity, cirrhosis, ethnic background, serum cytokine levels, liver fibrosis grades) [8], and treatment factors (adequate course of treatment, adherence to the treatment, management of side effects) [9] has been utilized in prior research to predict the outcome of combination therapy. Hepatic microRNA expression pattern before anti-viral treatment has also been utilized as a prediction biomarker of drug response in CH [10], while other studies have shown that there is a possible association between two SNPs near the gene interleukin 28B (IL28B) on chromosome 19 and lack of response to combination therapy [11–13].

In this study, we evaluated the IFN related gene expression profiles in CH patients before administering CH combination treatment. After the anti-viral therapy, patients were classified according to their clinical outcome: sustained viral response (SVR), relapse (R), and non responder (NR). It was observed that in the NR group, the expression level of some IFN related genes was significantly higher than that in normal liver (NL) groups, and that the expression level of the other IFN related genes was significantly lower than in NL. Moreover, the significantly high expression of IFN related genes was associated with low response to combination therapy. This suggests that dysregulation of the IFN system can be related to cases of CH combination therapy failure.

Results

In order to provide specific information with less data analysis, we developed a custom-made focused DNA microarray called Genopal (Mitsubishi Rayon, Tokyo, Japan) using genes that target human innate-immunity. Based on the results from the expression profiles, we carefully selected 237 gene probes (materials and methods) by activating RIG-I with Agilent DNA microarray. A microarray platform was used to establish IFN-related gene expression profiles in the specimens collected from the 87 CH and 5 NL samples (Table 1). The results of the analysis of these genes using the DNA chip strongly correlated with those obtained by real-time PCR (Pearson's correlation coefficient $R2 = 0.996$, $P<0.0001$; data not shown).

IFN related genes associated with the final response to combination therapy

We determined unique IFN gene expression patterns for liver specimens with or without HCV based on the final virological response to the combination therapy. The expression level of 66 genes significantly differed among NR, R, SVR, and normal liver (NL) groups (Figure 1). To clearly identify the IFN-related genes associated with the clinical outcome, we extracted genes that showed significant differences ($p<0.05$). It was observed that the expression level of 5 genes (myxovirus (influenza virus) resistance 1 (MX1), 2″,5″-oligoadenylate synthetase 1 (OAS1), ISG15 ubiquitin-like modifier (ISG15), interferon, alpha-inducible protein 27 (IFI27), and interferon, alpha-inducible protein 44 (IFI44)) were significantly higher in NR than in SVR samples (Table 2). The expression levels of 3 genes (MX1, IFI27, and ISG15) were significantly higher in NR than in R samples (Table 2). We also analyzed the IFN-related genes expression pattern according to the grade of inflammation or stage of fibrosis, however, no significant differences was observed between the two (data not shown).

Table 1. Clinical characteristics of patients.

Characteristics	SVR (n = 38)	R (n = 26)	NR (n = 23)	NL (n = 5)
Age	56.7±10.3	61.3±8.6	60.8±7.8	57.2±9.5
Male (%)	28 (61%)	11 (39%)	9 (36%)	3(60%)
Weight (kg)	59.5±8.9	57.2±10.3	55.7±7.2	ND
HCV RNA ($\times10^6$ copies/ml)	2.00±2.07	1.79±1.02	1.55±0.95	ND
Fibrosis stage				
F 0	1	1	1	
F 1	29	13	10	
F 2	9	7	5	
F 3	6	4	6	
F 4	0	0	1	
WBC($\times10^3$/mm^3)	5.42±1.63	5.23±1.25	4.69±1.13	ND
Hemoglobin (g/dl)	14.3±1.14	13.5±1.35	13.6±1.09	ND
Platelet ($\times10^4$/mm^3)	16.7±5.3	16.6±4.0	15.0±5.7	ND
AST (IU/L)	59.2±51.0	48.7±30.1	57.4±29.7	ND
ALT (IU/L)	80.8±93.7	49.3±29.6	69.1±44.4	ND
γGTP (IU/L)	60.3±74.2	41.2±29.7	76.2±60.2	ND
ALP (IU/L)	255±74.0	246±71.3	314±144	ND
Total bilirubin (mg/dl)	0.66±0.22	0.73±0.31	0.69±0.19	ND
Albumin (g/dl)	4.20±0.34	4.14±0.25	4.02±0.48	ND

Abbreviations; NR, non-virological responder; R, relapse; SVR, sustained virological responder; AST, aspartate aminotransferase;ALT, alanine aminotransferase; WBC, white blood cell; ALP, alkaline phosphatase; γGTP, gamma-glutamyl transpeptidase; ND, not detected.
doi:10.1371/journal.pone.0019799.t001

Comparison of IFN related genes between CH and NL

We also compared the gene expression pattern in NR and NL. After extracting genes with a fold change $<1/3$, $3<$ and p-value<0.05, we found that the expression level of 6 genes (growth arrest and DNA-damage-inducible, beta (GADD45B), hairy and enhancer of split 1 (HES1), B-cell CLL/lymphoma 3 (BCL3), signal transducer and activator of transcription 3 (STAT3), suppressor of cytokine signaling 3 (SOCS3), and DEAD/H (Asp-Glu-Ala-Asp/His) box polypeptide 11 (DDX11)) was significantly lower in NR than in NL. The expression level of SOCS3 and DDX11 in NR was significantly lower than in SVR. The expression level of 25 genes were significantly higher in NR than in NL. The expression levels of most of these genes were significantly higher in NR than in SVR, but the expression level of tumor necrosis factor (ligand) superfamily, member 10 (TRAIL), major histocompatibility complex, class I, C (HLA–C), major histocompatibility complex, class I, B (HLA–B), and chemokine (C-X-C motif) ligand 10 (CXCL10 (IP10)) were similar in NR and SVR samples (Table 3).

Validation of the microarray result by real-time qPCR

The five genes (ISG15, MX1, OAS1, IFI27 and IFI44) with the largest difference in fold change between NR and SVR groups were chosen to confirm the microarray results using real-time

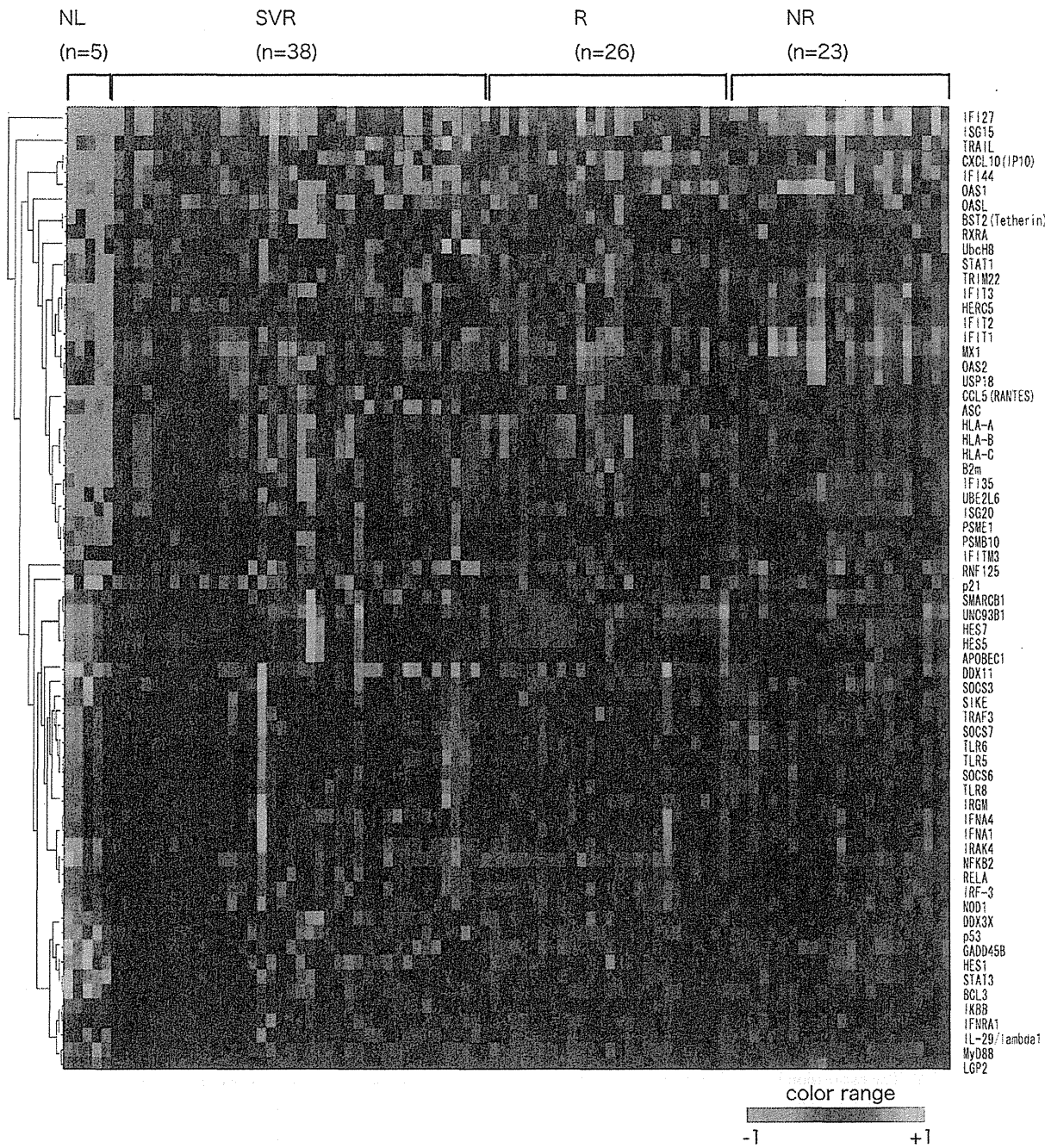

Figure 1. Clustering of IFN related gene expression. Clustering of CH patients according to the expression profiles of the 66 genes that showed significant differences among SVR, R, NR, and NL. Vertical bars represent the IFN related genes and the horizontal bars represent the samples. Green bars reflect down-regulated genes and red bars up-regulated genes.
doi:10.1371/journal.pone.0019799.g001

qPCR. The result from real-time qPCR supported the results from the microarray analysis (Figure S1).

Prediction of the clinical outcome by DLDA

We attempted to simulate the clinical outcome of the CH combination therapy using diagonal linear discriminant analysis (DLDA). Patients were randomly divided into TS (training set) and VS (validation set) (Table 4) in the order in which their samples were obtained. Samples within each group were then classified as NR or non-NR (SVR+R). DLDA showed that the accuracy, sensitivity, specificity, positive and negative predictive value of these two classifications were 86.1%, 87.5%, 81.8%, 93.3%, and

Table 2. Extracted genes related to the clinical outcome with a fold change greater than or equal to 1.5 between two groups (NR/SVR, NR/R) ($p<0.05$).

Accession No.	gene	symbol	fold change (NR/SVR)	p-value
NM_006417.4	interferon, alpha-inducible protein 44	IFI44	2.13	2.01E-03
NM_005532.3	interferon, alpha-inducible protein 27	IFI27*	2.37	2.01E-03
NM_016816.2	2″,5″-oligoadenylate synthetase 1, 40/46kDa, transcript variant 1	OAS1	2.51	1.36E-02
NM_005101.2	ISG15 ubiquitin-like modifier	ISG15*	2.68	1.18E-03
NM_002462.2	myxovirus (influenza virus) resistance 1, interferon-inducible protein p78 (mouse)	MX1*	2.71	1.57E-03
Accession No.	gene	symbol	fold change (NR/R)	p-value
NM_002462.2	myxovirus (influenza virus) resistance 1, interferon-inducible protein p78 (mouse)	MX1*	2.27	1.11E-03
NM_005532.3	interferon, alpha-inducible protein 27	IFI27*	2.33	1.69E-03
NM_005101.2	ISG15 ubiquitin-like modifier	ISG15*	2.5	1.11E-03

Asterisk deposits extracted genes that are common to both SVR and NR and to NR and R.
doi:10.1371/journal.pone.0019799.t002

69.2% respectively (Table 5). Additionally, we attempted to predict (1) SVR and nonSVR (R+NR), and (2) SVR, R, and NR by DLDA. The accuracy with which patients were classified as SVR and nonSVR, was 56.8% and as SVR, R, and NR was 56.9%.

Genetic variation of IL28B is correlated with the expression of IFN related genes

To examine the relationship between the genetic variation of IL28B and IFN related gene expression, we determined the IL28B polymorphism in 72 patients (Table 6). Patients with the minor genotype of IL28B displayed higher levels of hepatic ISGs expression, whereas patients with the major genotype showed significantly lower expression levels (Figure 2A). In order to further widen our understanding of the above relationship, we significantly identified individual genetic variations in IL28B at the clinical outcome (Figure 2B). We then individually compared the expression level of several IFN-lambda related genes at the clinical outcome with the genetic variation of IL28B. The expression level of interleukin 28A (IL28A), IL28B, interleukin 29 (IL29), interleukin 10 receptor, beta (IL10RB), signal transducer and activator of transcription 1 (STAT1), STAT5A, and tyrosine kinase 2 (TYK2) in IL28B genotype minor allele and major allele did not differ; however, the expression level of STAT5A and IRF9 was significantly higher in IL28B minor allele cases than in major allele (Figure 3A). The expression levels of these nine genes did not significantly differ among the clinical outcomes (NR, R, and SVR) (Figure 3B).

Finally, in regards to genes which contribute to IFN production (interferon regulatory factor 7 (IRF7), interleukin-1 receptor-associated kinase 1 (IRAK1), myeloid differentiation primary response gene (MyD88), and toll-like receptor 7 (TLR7)) there was not much difference in their expression level prior to CH combination treatment and their expression level at the clinical outcome (Figure 4A) [14]. Unlike IRF7 and MyD88, there was no significant difference in the expression level of IRAK1 and TLR7 according to the IL28B genetic variation (Figure 4B). When we attempted to predict NR and nonNR by using ISG genes with and without IL28B polymorphism using DLDA by using 72 patients (36 patients for training set, 36 patients for validation set). DLDA with IFN related gene and IL28B polymorphism showed that the accuracy, sensitivity, specificity, positive and negative predictive value of these two classifications were 83.3%, 85.1%, 77.8%, 92.0%, 63.6%, respectively (Table 7). DLDA with IFN related gene only showed that the accuracy, sensitivity, specificity, positive and negative predictive value were 83.3%, 81.5%, 88.9%, 95.7%, 61.5%, respectively (Table 8).

Discussion

Our comprehensive analysis identified 66 genes with expression levels that consistently differed depending on the drug response of 87 CH patients and 5 normal liver specimens (Figure 1). Comparing the gene expression pattern in NR and NL showed the expression levels of 31 genes were significantly different (Table 3). In addition, most genes with expression levels in NR that were higher or lower than in NL, also differed between NR and SVR. Therefore, it is possible that innate immunity in the early period of HCV infection strongly influences IFN reaction.

HCV infection induces the impairment of cell subset number and the function of plasmacytoid dendritic cells (PDC) and natural killer cells [15]. The amount of PDC, which are the most potent producers of antiviral Type-I and III IFN [16], decreased in patients' peripheral blood [17], however, PDC was trapped in the HCV infected liver tissue. Therapeutic non-responders had increased PDC migration to inflammatory chemokines before therapy, compared with therapeutic responders [18]. This situation resulted in elevated expressions of IFN-related genes in the CH samples and was associated with their inability to eliminate the virus [19].

Inadequate expression of IFN related genes has been associated with several diseases. High expression of ISG can induce a refractory state in IFN therapy [20] and impaired IFN production leads to high risk of HCV-related hepatocarcinogenesis [21]. Lymphocyte IFN signaling was less responsive in patients with breast cancer, melanoma, and gastrointestinal cancer and these defects may represent a common cancer-associated mechanism of immune dysfunction. Alternately, since immunotherapeutic strategies require functional immune activation, such impaired IFN signaling may hinder therapeutic approaches designed to stimulate anti-tumor immunity [22]. In this way, the dysregulation of the IFN system can influence the progression of diseases and decrease curative effects.